minerals

Article

Eoarchean to Neoproterozoic Detrital Zircons from the South of Meiganga Gold-Bearing Sediments (Adamawa, Cameroon): Their Closeness with Rocks of the Pan-African Cameroon Mobile Belt and Congo Craton

Nguo Sylvestre Kanouo [1,*], Arnaud Patrice Kouske [2], Gabriel Ngueutchoua [3], Akella Satya Venkatesh [4], Prabodha Ranjan Sahoo [4] and Emmanuel Archelaus Afanga Basua [5]

[1] Department of Mining Engineering and Mineral Processing, Faculty of Mines and Petroleum Industries, University of Maroua, Maroua 46, Cameroon
[2] Department of Civil Engineering, University Institute of Technology (UIT), University of Douala, Douala 1623, Cameroon; arnaudpatricek@gmail.com
[3] Department of Earth Sciences, University of Yaoundé I, Yaoundé 812, Cameroon; ngueutchoua2@yahoo.fr
[4] Department of Applied Geology, Indian Institute of Technology (Indian School of Mines), Dhanbad 826004, India; asvenkatesh@iitism.ac.in (A.S.V.); prabodha@iitism.ac.in (P.R.S.)
[5] Faculty of Earth Sciences, School of Earth Sciences, China University of Geosciences, Wuhan 430074, China; basfanga@yahoo.com
* Correspondence: sylvestrekanouo@yahoo.fr; Tel.: +237-678966240

Abstract: The core of detrital zircons from the southern Meiganga gold-bearing placers were analyzed by Laser Ablation Split Stream analytical techniques to determine their trace element abundances and U-Pb ages. The obtained data were used to characterize each grain, determine its formation condition, and try to trace the provenance. The Hf (5980 to 12,010 ppm), Y (27–1650 ppm), U (25–954 ppm), Th (8–674 ppm), Ti (2–256 ppm), Ta, Nb, and Sr (mainly <5 ppm), Th/U (0.06–2.35), Ti zircon temperature (617–1180 °C), ∑REE (total rare earth element) (98–1030 ppm), and Eu/Eu* (0.03 to <1.35) are predominant values for igneous crustal-derived zircons, with very few from mantle sources and of metamorphic origin. Crustal igneous zircons are mainly inherited grains crystallized in granitic magmas (with some charnockitic and tonalitic affinities) and a few from syenitic melts. Mantle zircons were crystallized in trace element depleted mantle source magmatic intrusion during crustal opening. Metamorphic zircons grown in sub-solidus solution in equilibrium with garnet "syn-metamorphic zircons" and in equilibrium with anatectic melts "anatectic zircons" during crustal tectono-metamorphic events. The U-Pb (3671 ± 23–612 ± 11 Ma) ages distinguish: Eoarchean to Neoproterozoic igneous zircons; Neoarchean to Mid Paleoproterozoic anatectic zircons; and Late Neoproterozoic syn-metamorphic grains. The Mesoarchean to Middle Paleoproterozoic igneous zircons are probably inherited from pyroxene-amphibole-bearing gneiss (TTGs composition) and amphibole-biotite gneiss, whose features are similar to those of the granites, granodiorites, TTG, and charnockites found in the Congo Craton, south Cameroon. The youngest igneous zircons could be grains eroded from Pan-African intrusion(s) found locally. Anatectic and syn-metamorphic zircons could have originated from amphibole-biotite gneiss underlying the zircon-gold bearing placers and from locally found migmatized rocks that are from the Cameroon mobile belt, which could be used as proxies for tracking gold.

Keywords: Cameroon; Meiganga; gold placer; detrital zircon; trace element; geochronology; Archean-Proterozoic origins

Citation: Kanouo, N.S.; Kouske, A.P.; Ngueutchoua, G.; Venkatesh, A.S.; Sahoo, P.R.; Basua, E.A.A. Eoarchean to Neoproterozoic Detrital Zircons from the South of Meiganga Gold-Bearing Sediments (Adamawa, Cameroon): Their Closeness with Rocks of the Pan-African Cameroon Mobile Belt and Congo Craton. *Minerals* **2021**, *11*, 77. https://dx.doi.org/10.3390/min11010077

Received: 30 August 2020
Accepted: 11 November 2020
Published: 15 January 2021

Publisher's Note: MDPI stays neutral with regard to jurisdictional claims in published maps and institutional affiliations.

Copyright: © 2021 by the authors. Licensee MDPI, Basel, Switzerland. This article is an open access article distributed under the terms and conditions of the Creative Commons Attribution (CC BY) license (https://creativecommons.org/licenses/by/4.0/).

1. Introduction

Meiganga is one of the key areas for small scale gold mining activities in Cameroon. As in many areas in this country, gold is extracted from supergene assemblages and terrigenous sediments (alluvium, eluvium, colluvium, and terrace) of mostly unknown primary sources (Figure 1). The clastic gold particles (very fine to coarse grained) are generally associated with some heavy minerals (e.g., zircon, magnetite, kyanite, ilmenite, and tourmaline) [1,2]. These weathering-resistant minerals are very useful in provenance studies, as they can register important information on their source rock petrogenesis, paleoenvironment, and tectonic reconstitution [3–9]. Some of these heavy minerals often fingerprint information on the chemistry of their environment of crystallization, the nature of their source rocks, and on the pre-existing tectonic settings [4,5,8–11]. Zircon in particular is an important mineral in fingerprinting source parameters [5,12–15]. One of the key tools to determine zircon source parameters is the combination of zircon geochemistry and U-Pb dating [4,8–10]. Each zircon has a characteristic age reflecting its genesis, and the population of detrital zircons in a sediment is a function of the age signature of source rocks in the proto-source terranes [12].

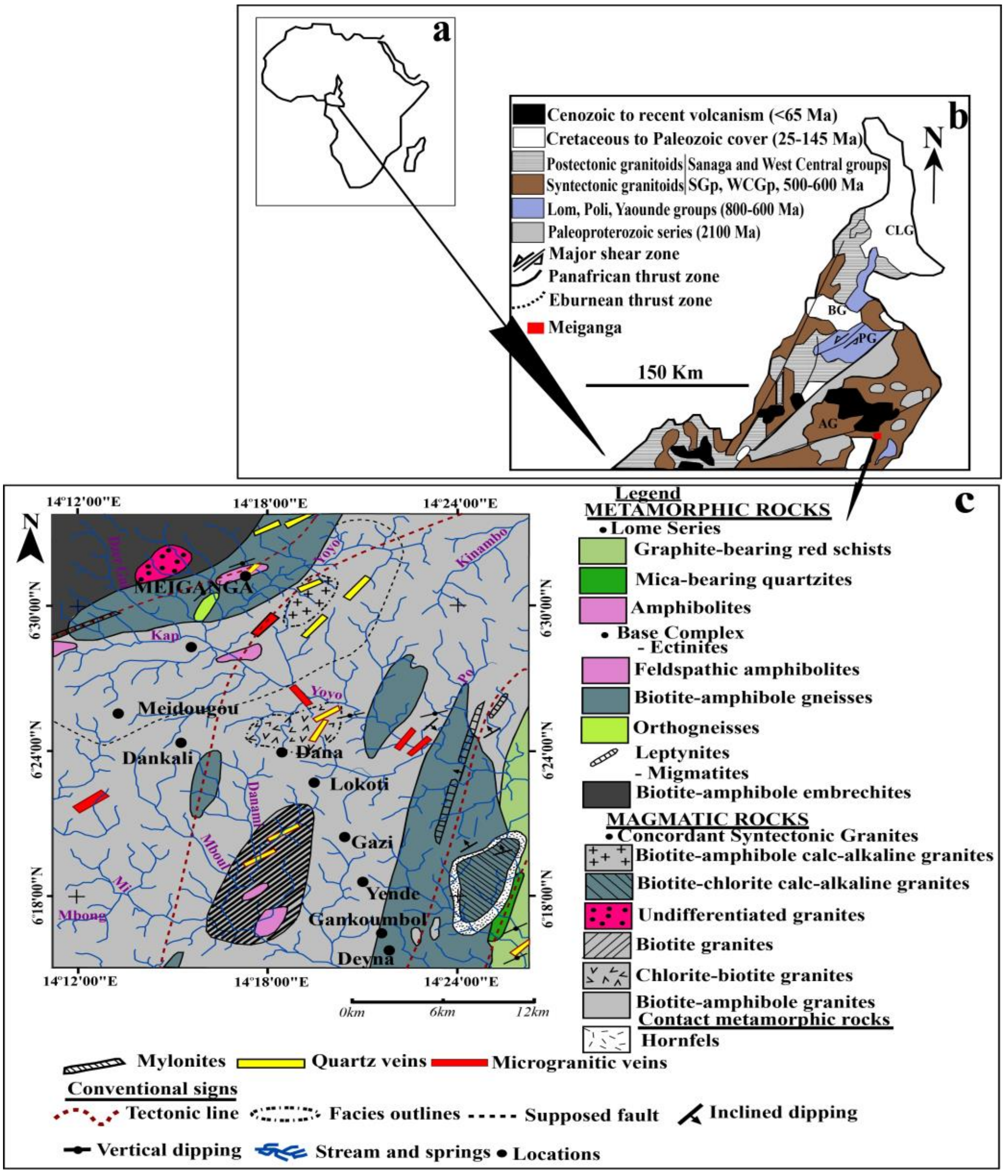

Figure 1. Geological sketch map of regional and local settings; (**a**) Cameroon in Africa, (**b**) geologic map of Adamawa, North and Far North Cameroon with the location of the south of Meiganga and (**c**) geological map of the south of Meiganga with the sample location.

Meiganga is in the Central part of the Cameroon mobile belt [16], a mega-tectonic structure that formed during the Neoproterozoic, from a collision between the Saharan meta-craton and Congo Craton [17,18]. Recent research works carried out on rocks found in the west of Meiganga have revealed the existence of Archean and Paleoproterozoic inheritance [19–21]. Trace element geochemistry and U-Pb ages of detrital zircon from gold-bearing placers in the west of Meiganga show that they were mainly crystallized and sourced from Archean to Precambrian granitoids [9].

Gold-bearing sediments were found in some streams in the southern part of Meiganga. The gold particles are associated with zircon, tourmaline, magnetite, kyanite, and ilmenite [1]. The source rocks and crystallization processes of most of these heavy minerals are poorly constrained. Djou [1] suggested a gneissic origin for a part of the deposited clasts, based on the presence of kyanite within the heavy mineral suites. Detailed analyses have not yet been carried on those minerals to help understand their source history and constrain their provenance. In this paper, we present trace element abundance and U-Pb core age for zircons from this gold placer. These data are used to characterize each grain, understand its formation history, and try to locate its proto-source and source rock within the local and regional settings.

2. Overview on the Regional and Local Geologic Settings

2.1. Brief Review of the Regional Geology

Basement formations in Cameroon (Figure 2) comprise Archean, Paleoproterozoic (Eburnean), and Pan-African rocks (Table 1). Archean units (>2500 Ma) constitute the Congo Craton, while the Paleoproterozoic ones (2400–1800 Ma) include the West Central African Belt and Pan-African/Cambrian units that constitute the Oubanguide Belt in the Mobile Zone [22,23].

2.1.1. The Ntem Complex

The Archean Craton or Ntem Complex (Figure 2) located in the northwestern end of the Congo Craton [24] is mainly composed of Archean rocks (Table 1) with some reworked Paleoproterozoic material that formed in early Proterozoic times [25]. It is structurally made up of two main units: the Ntem (at the center and south) and the Nyong (in the northwestern) [24]. The Ntem unit is essentially made up of tonalite, trondhjemite, and granodioritic suites (TTGs) and charnockites with TTGs cutting across charnockites and greenstone belts [26]. TTGs and charnockites enclose xenolithic remnants (3.1 Ga) of greenstone belts (banded iron formations and sillimanite-bearing paragneisses) [27,28]. Bounded Iron Formations found in the Ntem unit are locally intercalated with meta-siltstones and meta-sandstones [29]. The TTGs and charnockites were intruded by K-rich granitoids (monzogranite and syenogranite) during the Archean [30,31] and cross-cut by metadoleritic dykes during the Eburnean [32,33] or Late Archean time [34]. The Nyong unit, ranging in age from Archean to Paleoproterozoic [32,35–37], and part of the West Central African Fold Belt [23], is composed of migmatitic orthogneisses (TTGs), meta-gabbro, amphibolite, garnetite, eclogite, felsic gneiss of volcanic to volcano-sedimentary origin, quartzite, charnockite, meta-syenite, and BIF [22,23,37]. Migmatites, charnockites, and meta-sedimentary rocks are Archean in age [32,35].

Table 1. Summarized ages of plutonic and metamorphic rocks found in Congo Craton, Cameroon mobile belt, and Meiganga.

Regional Scale						Local Scale	
Congo Craton (Ntem Complex)				Cameroon Mobile Belt			
Ntem Unit		Nyong Unit					
Rock Type	**Age and Author(s)**	**Rock Type**	**Age and Author(s)**	**Rock Type**	**Age and Author (s)**	**Rock Type**	**Age and Author (s)**
Charnockites (north of the Ntem unit)	2900 ± 44 and 2818 ± 48 Ma (Rb/Sr [39])	Magnetite-bearing quartzites (BIF) in Eseka	2776 ± 34 Ma and 2126 ± 136 Ma (SHRIMP U-Pb zircon: [37])	Panafrican granitoids	Poli (520 ± 20 Ma) and Lom (498 ± 5 (Ma) (Rb-Sr age on whole –rock, [35]) Nkambe (530 ± 10 Ma and 510 ± 25 Ma; 569 ± 12 to 558 ± 24 Ma, and 533 ± 12 to 524 ± 28 Ma) [40,41] Ngondo (600 Ma) [42] Tonga (618 Ma) [43]	Pyroxene-amphibole-bearing gneiss (TTG composition) (SW of Meiganga)	1711.7 ± 4 to 2602.2 ± 13.6 Ma ($^{207}Pb/^{206}Pb$ zircon evaporation: [44]) 1738 ± 14 to 2987 ± 28 Ma ($^{206}Pb/^{238}U$) 1999 ± 2 to 2884 ± 4 Ma ($^{207}Pb/^{206}Pb$) [20]
Charnockites (north of the Ntem unit)	2882 ± 70 Ma (Rb/Sr: [32]) 2912 ± 25 Ma ($^{207}Pb/^{206}Pb$ zircon evaporation: [26])	Garnet-bearing gneiss in Eseka	2761–2790 Ma (SHRIMP U-Pb zircon: [37])	Granulite in Yaoundé	620 ± 10 Ma [45]	Amphibole-biotite gneiss	1887 to 2339.4 Ma and 675 to 889 Ma ($^{207}Pb/^{206}Pb$ zircon evaporation: [19])
Charnockites (Ebolowa)	2896 ± 7 Ma (U/Pb zircon: [32])	Kribi metquartzites	2948 ± 47 Ma and 2049 ± 36 Ma (U-Pb zircon: [32])	Monzodiorite in Bafia	600 Ma [46]	Metadiorite (NE of Meiganga)	614.1 ± 3.9 Ma and 619.8 ± 9.8 Ma ($^{207}Pb/^{206}Pb$ zircon evaporation: [47]) 562 ± 6 to 637 ± 5 Ma (U-Pb zircon: [48])
Charnockites (Sangmelima)	3010 ± 10 to 2756 ± 14 Ma ($^{207}Pb/^{206}Pb$ zircon evaporation: [49])	Amphibolite in Eseka	2000–2010 Ma (U-Pb zircon: [32])	Metasediments in Bafia	1617 ± 16 [36]	Two micas granite in Doua (West of Meiganga)	647 ± 46 Ma (U-Pb zircon: [21])

Table 1. *Cont.*

Regional Scale						Local Scale	
Congo Craton (Ntem Complex)				Cameroon Mobile Belt			
Ntem Unit		Nyong Unit					
Rock Type	**Age and Author(s)**	**Rock Type**	**Age and Author(s)**	**Rock Type**	**Age and Author (s)**	**Rock Type**	**Age and Author (s)**
Tonalites (Sangmelima)	2825 ± 11 to 2678 ± 17 Ma ($^{207}Pb/^{206}Pb$ zircon evaporation: [49])	Amphibolite in Kopongo	2037± 10 Ma and 626 ± 26 Ma Ma (U-Pb zircon: [32])	-	-	Amphibole-biotite granite in Doua (West of Meiganga)	607 ± 3.9 (U-Pb zircon: [21])
Granodiorites (Sangmelima)	2999 ± 10 to 2671 ± 25 ($^{207}Pb/^{206}Pb$ zircon evaporation: [49])	Orthopyroxene-garnet geneiss (charnockitic) Eseka	3174 ± 4 Ma, 3129 ± 10 Ma, 3064 ± 4 Ma 2086 ± 8 Ma, 2300 ± 17 Ma (SHRIMP U-Pb zircon: [37])	-	-	-	–
High-K granites (Sangmelima)	2717 ± 9 to 2724 ± 3 Ma ($^{207}Pb/^{206}Pb$ zircon evaporation: [31])	Bienkok charnockite	2051 ± 10 Ma and 2043 ± 22 Ma (SHRIMP U-Pb zircon: [37])	-	-	-	-
Granodiorites	2880 ± 70 Ma (Rb/Sr isochrones: [35])	Bonguen metagranodiorites	2066 ± 4 Ma (SHRIMP U-Pb zircon: [37])	-	-	-	-
Granodiorites (north of the Ntem unit)	2.97 Ga ($^{207}Pb/^{206}Pb$ zircon evaporation: [26])	Rocher du Loup Panafrican metasyenites	591 ± 19Ma (SHRIMP U-Pb zircon: [37])	-	-	-	–
Tonalites (north of the Ntem unit)	3.10–2.97 Ga ($^{207}Pb/^{206}Pb$ zircon evaporation: [26])	Lolodorph metasyenites	2055 ± 5 Ma (SHRIMP U-Pb zircon: [37])	-	-	-	-
Pyroxene-bearing gneisses	2980 ± 45 Ma (Rb/Sr isochrones: [35])	Nkonlong and Akom syenites	525 and 807 Ma (K/Ar dating on hornblende: [50])	-	-	-	-
Xenoliths from greenstone belts	3.1 Ga ($^{207}Pb/^{206}Pb$ zircon evaporation: [28])	Lolodorf-Doum clinopyroxene syenites	2837 ± 1–2349 ± 1 ($^{207}Pb/^{206}Pb$ zircon evaporation: [51])	-	-	-	-

Table 1. *Cont.*

Regional Scale						Local Scale	
Congo Craton (Ntem Complex)				Cameroon Mobile Belt			
Ntem Unit		Nyong Unit					
Rock Type	**Age and Author(s)**	**Rock Type**	**Age and Author(s)**	**Rock Type**	**Age and Author (s)**	**Rock Type**	**Age and Author (s)**
K-rich granitoids (Ebolowa)	2.7–2.5 Ga (^{207}Pb/^{206}Pb zircon evaporation: [25])	-	-	-	-	-	-
Metadoleritic dykes	2.1 Ga (U-Pb zircon: [32])	-	-	-	-	-	-
Mengueme two pyroxenes syenites	2321 ± 1 (^{207}Pb/^{206}Pb Pb–Pb zircon evaporation: [51])	-	-	-	-	-	-
Njweng metasandstone (Mbalam iron ore)	3000–1000 Ma [29]	-	-	-	-	-	-

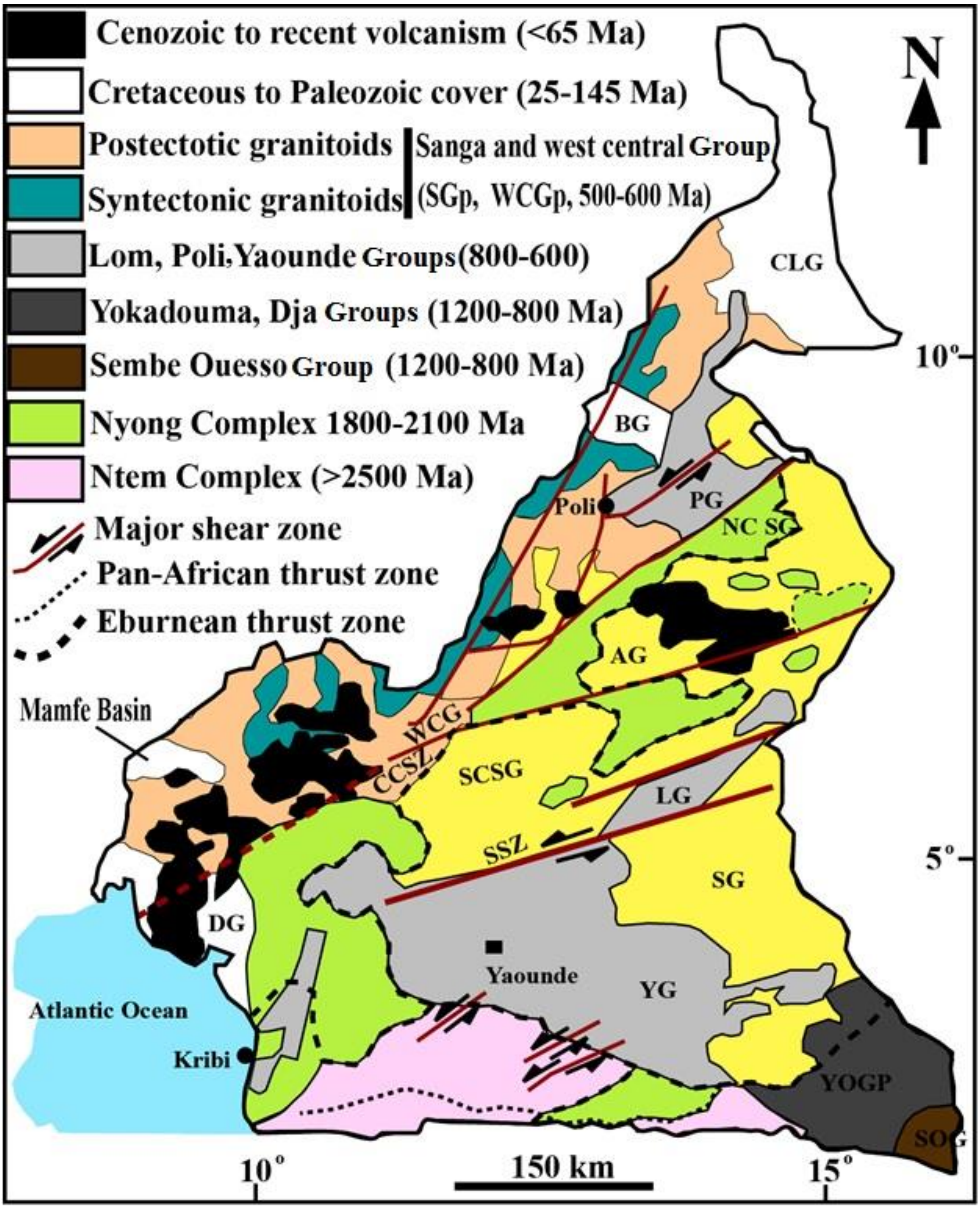

Figure 2. Sketch geological map of Cameroon (adapted from [38]). Oubanguide Complex: NCSG: Northern Cameroon SGp (PG: Poli Group, AG: Adamawa Group, WCG: West Cameroon Group); SCSG: Southern Cameroon SGp (YG: Yaoundé Group, LG: Lom Group, SG: Sanaga Group); SECSGp: Southeastern Cameroon SGp (DG: Dja, YoGroup: Yokadouma, S.O.Group: Sembe Ouesso Group); CCSZ: Centre Cameroon shear zone; SSZ: Sanaga shear zone; Sedimentary cover: (CLG: Chad Lake Group; BG: Benue Group; MG: Manfe Group; DG: Douala Group); B: Cameroon main litho-structural units.

2.1.2. The Cameroon Mobile Belt

The Cameroon mobile zone or Central African Fold belt is a mega-tectonic structure underlying Cameroon, Chad, and the Central African Republic between the Congo Craton to the south and the Nigerian shield to the north [52]. It was formed during the Neoproterozoic, from the collision between the Saharan meta-craton and the Congo craton [17,18]. In the Cameroonian territory, the Central African Fold belt is made up of three main structural units: the Poli Group in its northern part, the Adamawa at the center, and the Yaoundé Group in the south [18]. Within the central African fold belt, several domains are recognized on the basis of field, petrographic, structural, and isotopic studies. These include the Paleoproterozoic gneissic basement, Mesoproterozic to Neoproterozoic schists, and gneisses of Poli, Yaoundé, and Lom, and Pan-African granitoids whose ages range from the early stage of the deformation (orthogneisses) to the late uplit stages of the belts [36]. Examples of geochronological data of some of these rocks are summarized in Table 1.

2.2. Local Geology

The Meiganga part of the Adamawa-Yadé domain (AYD) (Figure 2) is situated between the Congo Craton and the Sahara Metacratron [20]. Basement rocks in Meiganga are composed of paragneisses, orthogneisses, amphibolites, granulites, migmatites, quartzites, metadiorites, schists, and granites [1,2,16,21]. Some gneisses and amphibolites underwent retrograde metamorphism that led to the formation of greenschist facies overprints [16]. Partial melting of gneiss led to the crystallization of leucogranites found in the northern part of Meiganga [16]. Magmatism, cataclastic deformation, rock fracturing, and partial melting of some basement rocks led to the formation of mafic dykes and dykelets, syenitic, micro-granitic, quartzo-feldspathic and quartz-rich veins, brecciated shear zones, and mylonites [1,2,16]. The basement rocks are locally overlain by basaltic flows, lithified clastic sediments (sandstones and conglomerates), unconsolidated detritus (e.g., colluvium, eluvium, alluvium), or red soil [1,2,53]. Skarnoids (hornfels) are visible at the contact between some intrusions and overlying sedimentary rocks.

The western part of Meiganga is made up of pyroxene-amphibole orthogneiss, amphibole gneiss, biotite gneiss, amphibole-biotite gneiss, amphibolite, calc-alkaline and two mica-granites, and amphibole-biotite granite [16,19–21,44,47,53]. Pyroxene-amphibole orthogneiss locally enclose mafic xenoliths [44]. The geochemical features of the orthogneiss and U-Pb zircon ages are similar to those of many TTGs and charnockites outcropping within the Archean Ntem complex in the south of Cameroon [20,44]. The ages of some rocks in the west of Meiganga presented in Table 1 range from Archean to Neoproterozoic. Zircons occurring in a gold-bearing placer in the west of Meiganga are inherited grains crystallized from Archean to Precambrian magmatic crustal evens with part of their source rocks being granitoids, TTG, and charnockites [9].

The southern part of Meiganga (Figure 1c) from where the studied zircon were sampled are composed of mainly undated graphite schists, amphibolites, mica-rich quartzites, amphibole-biotite gneisses, orthogneisses, migmatites, calc-alkaline granitic rocks, biotite-amphibole, and biotite-chlorite granites whose formation periods are assumed to be Precambrian as they also belong to the central part of the Cameroon mobile belt [53]. Hornfels are found at the contact between calc-alkaline biotite-chlorite granite and biotite-chlorite granite at the south eastern part of the locality (Figure 1c). Rocks found in valleys are locally covered by alluvial flats and terraces with part of the alluvium hosting gold.

3. Materials and Methods

In total, 111 zircons from gold-bearing alluviums in two areas (Gankoumbol and Yende: Figure 1) were analyzed to determine the trace elements composition and U-Pb core age at the University of California, Santa Barbara, CA, USA. The results from each zircon core were acquired by Laser Ablation Split Stream analytical techniques. The analyzed zircons were sampled upstream and in small size streams to be close to the source area.

They were separated from pre-concentrated heavy and light minerals mixtures obtained from 50 L of mainly very coarse-grained alluvium, at the bottom of the gold-bearing pits. Heavy mineral fractions were separated from light minerals using bromoform (Density: 2.7 g/cm^{-3}) at the Department of Earth Sciences of the University of Yaoundé I, Cameroon. The separation procedure is similar to the one described in [54,55].

The gold-bearing heavy mineral fractions were sent for zircon separation, trace element analysis, and U-Pb dating at the Department of Earth Sciences of the University of California. The analytical procedures used to obtain the zircon trace element and U-Pb age data are the same as those presented in [9]. Each mounted grain is polished and analyzed following standard procedures using a laser ablation "split stream" setup consisting of a Photon Machines Excimer 193 nm laser ablation unit coupled to a Nu Instruments, "Nu Plasma" multi-collector inductively coupled a plasma-mass spectrometer and an Agilent 7700S quadrupole inductively coupled plasma-mass spectrometer (for detailed methodology see [56–58]. Samples were abraded for 20 s using a fluence of 1.5 J/cm^2, a frequency of 4 Hz, and a spot size of 20 µm diameter, resulting in crater depths of ~9 µm. Utilizing a standard-sample bracketing technique, analyses of reference materials with known isotopic compositions were measured before and after each set of the seven unknown analyses. Data reduction, including corrections for baseline, instrumental drift, mass bias, down-hole fractionation, and age and trace element concentration calculations were carried out using Iolite v. 2.1.2 [59]. "91500" zircon (1065.4 ± 0.3 Ma $^{207}Pb/^{206}Pb$ ID-TIMS age and 1062.4 ± 0.4 Ma $^{206}Pb/^{238}U$ ID-TIMS age: [60]) served as the primary reference material to monitor and correct for mass bias, as well as Pb/U down-hole fractionation and to calibrate concentration data, while "GJ-1" zircon (608.5 ± 0.4 Ma $^{207}Pb/^{206}Pb$ and 601.7 ± 1.3 Ma $^{206}Pb/^{238}U$ ID-TIMS ages: [61]) was treated as an unknown in order to assess accuracy and precision. Twenty-three analyses of GJ-1 zircon throughout the analytical session yield a weighted mean $^{207}Pb/^{206}Pb$ date of 593 ± 5 Ma, MSWD = 0.8 and a weighted mean $^{206}Pb/^{238}U$ date of 603 ± 2 Ma, MSWD = 1.0. Concordia and Kernal Density Estimate (KDE) plots were calculated in Isoplot version 2.4 [62] and Density Plotter [63], respectively, using the ^{238}U and ^{235}U decay constants of [64]. All uncertainties are quoted at 95% confidence levels or 2 s level and include contributions from the external reproducibility of the primary reference material for the $^{207}Pb/^{206}Pb$ and $^{206}Pb/^{238}U$ ratios. For plotting and age interpretation purposes, the $^{207}Pb/^{206}Pb$ dates are used for analyses older than 1000 Ma, whereas the $^{206}Pb/^{238}U$ dates are used for analyses younger than 1000 Ma.

4. Results

4.1. Zircon Geochemistry

4.1.1. Minor Elements

The relatively high Y and Hf contents in part of the studied zircons can reflect a crystallization in Hf-Y-rich melts with favorable conditions for Hf and Y to substitute Zr. The Hf/Y ratios (5.0−293.0) are mainly less than 30, with the highest values exclusively being those of zircons with very low Y contents.

4.1.2. Trace Elements

The trace element (U, Th, Ti, Ta, Nb, Pb, and Sr) abundances (<1000 ppm) and Th/U ratios are heterogeneous with similar values found in some grains (Tables 2 and 3). Within U and Th elemental suites, U contents (25−954 ppm) mainly exceed 219 ppm, and Th contents (8–674 ppm) are mostly greater than 100 ppm. The Th/U ratios (0.06 to >2.0) are larger than 0.4. Four groups can be distinguished (Figure 3): (1) zircons with Th/U ratios (<0.2) (lowest proportion); (2) zircons with Th/U ratios (≥0.2 to ≤0.5) (highest proportion); (3) zircons with Th/U ratios (>0.5 to ≤1.0); and (4) zircons with Th/U ratios >1.0. The plotted data in Th versus U binary diagram (Figure 4a) show a pronounced positive correlation (the increase in U content when Th content increases) for group 2–4 zircons; however, no correlation is found for group 1 zircons, as their plots are scattered. This correlation is less pronounced (as part of the plots are scattered) in the Th/U versus U(Figure 4b) and Th/U versus Th (Figure 4c) plot diagrams. The Th/U ratios for group 2 to group 4 are within the range of igneous zircons as presented in [4,5,11,65,66]. Those of group 1 (e.g., MSDZ015, MSDZ040, MSDZ045, MSDZ067, MSDZ082, and MSDZ093) characterize metamorphic zircons if based on the criteria of [5], [67], and [68].

Table 2. Minor and trace element concentrations (ppm) in the southern Meiganga detrital zircons.

Sample Spot-Name	Hf	Th	Ti	Ta	Nb	Sr	Hf/Y	Nb/Ta	Ti-in-Zircon T (°C) ± 2σ	
MSDZ001	10,750	154	8.7	1.16	1	0.11	38.256	0.842	733	50
MSDZ002	7820	79	30	1.56	2.2	0.27	5.6259	1.421	861	88
MSDZ003	7210	48	7.3	0.46	0.6	0.18	7.2755	1.202	717	79
MSDZ004	9860	341	10	3.46	3.3	0.18	10.956	0.966	746	40
MSDZ005	10,260	177	20.9	1.75	2.1	7.22	18.127	1.222	820	76
MSDZ006	8930	165	8.9	1.92	1.8	0.22	13.696	0.961	735	66
MSDZ007	6750	16	6	0.35	0.6	0.15	12.546	1.848	700	60
MSDZ008	11,440	268	47	1.78	2.3	0.31	21.749	1.283	915	135
MSDZ009	7090	70	9.8	0.16	0.5	0.11	10.381	3.315	744	87
MSDZ010	8910	230	8.1	1.06	1.4	0.15	35.217	1.303	726	71
MSDZ011	8310	217	14.8	1.23	1.5	0.23	13.317	1.18	784	102
MSDZ012	7600	42	2.5	0.59	0.9	0.14	15.05	1.58	630	84
MSDZ013	11,390	299	16.3	1.54	1.1	0.03	54.76	0.7	794	44
MSDZ014	11,520	116	11	0.35	0.4	1.86	44.24	1.213	755	61
MSDZ015	10,380	123	10.9	2.19	1.8	0.31	18.703	0.831	754	39
MSDZ016	5960	12	10.7	0.37	0.3	0.08	21.06	0.885	752	60
MSDZ017	9630	217	7.1	3.53	3.8	0.16	14.038	1.085	715	54
MSDZ018	7030	44	5	0.75	1.1	0.16	7.8547	1.53	685	98
MSDZ019	7500	22	6.1	0.65	0.9	0.17	13.915	1.316	701	63
MSDZ020	7040	38	10.1	0.27	0.4	0.09	22.564	1.603	747	51
MSDZ021	9110	87	5.4	1.33	1.5	0.16	14.717	1.155	691	65
MSDZ022	9110	264	6.5	3.91	4.6	0.2	11.016	1.169	707	74
MSDZ023	9190	253	11.6	1.58	2.2	0.07	22.36	1.397	760	50
MSDZ024	9630	161	7	3.44	3.6	0.16	14.658	1.041	713	68
MSDZ025	10,340	269	35.7	0.76	0.9	1.36	26.649	1.24	881	48
MSDZ026	9570	263	8.1	3.17	4.4	0.19	9.071	1.394	726	76
MSDZ027	10,520	155	8	2.25	2.8	0.14	23.223	1.259	725	79
MSDZ028	10,470	155	10.1	3.11	3.9	0.11	21.904	1.25	747	69
MSDZ029	7480	22	3.6	0.32	0.4	0.07	19.947	1.187	658	122
MSDZ030	7790	70	7.9	1.44	0.8	0.03	292.857	0.58	724	70
MSDZ031	7760	9	5.4	0.14	0.3	0.08	26.667	2.385	691	75
MSDZ032	7470	78	10	1.12	1	0.13	14.792	0.868	746	61
MSDZ033	9030	71	6.7	2.33	2.2	0.21	16.329	0.958	710	40
MSDZ034	9020	19	5.2	0.63	0.9	0.11	21.683	1.355	688	56
MSDZ035	9080	466	25.8	2.25	1.6	0.14	10.425	0.703	843	42
MSDZ036	8360	160	7.2	0.75	0.5	0.16	23.158	0.726	716	77
MSDZ037	10,630	298	8.6	1.6	2.1	0.14	15.842	1.311	732	46
MSDZ038	8700	16	5.2	0.46	0.8	0.09	30.742	1.659	688	50
MSDZ039	8090	266	11.8	1.14	1.5	0.07	16.116	1.338	762	72
MSDZ040	8910	13	3.5	0.16	0.3	0.09	26.053	2.056	656	60
MSDZ041	10,120	334	19	1.32	2.2	0.14	10.87	1.681	810	40
MSDZ042	9560	334	8.2	2.09	3.5	0.15	14.914	1.669	728	49
MSDZ043	8790	97	15.8	0.51	1	0.18	10.68	1.883	791	61
MSDZ044	9150	91	35.9	0.26	0.4	0.05	48.93	1.53	882	66
MSDZ045	7100	45	2.5	0.77	0.8	0.12	9.9162	1.089	630	84
MSDZ046	9790	26	5.3	1.76	1.1	0.04	63.161	0.637	690	59
MSDZ047	9680	180	9.9	1.24	1.6	0.08	40.844	1.295	745	54
MSDZ048	9630	203	6.2	2.66	3.5	0.19	10.201	1.327	703	62
MSDZ049	9960	145	20.9	1.8	1.7	0.1	39.059	0.965	820	97
MSDZ050	7980	36	2.7	0.46	0.8	0.16	12.587	1.702	636	73
MSDZ051	11,750	100	5.6	1.67	1.8	0.18	11.75	1.064	694	73

Table 2. *Cont.*

Sample Spot-Name	Hf	Th	Ti	Ta	Nb	Sr	Hf/Y	Nb/Ta	Ti-in-Zircon T (°C) ± 2σ	
MSDZ052	9930	347	7.1	4.43	4.4	0.23	14.56	0.982	715	78
MSDZ053	10,450	122	11.5	0.68	1	0.07	51.225	1.412	759	56
MSDZ054	8030	91	6.7	0.46	1.5	0.28	6.323	3.213	710	67
MSDZ055	9810	153	256	1.23	2.9	15.99	15.046	2.393	1180	47
MSDZ056	10,190	363	4.4	1.93	2	0.2	8.291	1.032	674	48
MSDZ057	8230	20	6.4	0.38	0.5	0.07	32.789	1.38	706	49
MSDZ058	9990	208	6	2.66	4.1	0.2	8.339	1.534	700	60
MSDZ059	10,110	138	7.5	0.71	1.3	0.02	273.984	1.842	720	57
MSDZ060	8710	19	3	0.44	0.4	0.12	16.75	0.913	644	60
MSDZ061	10,540	17	2.1	0.6	0.4	0.09	57.127	0.747	618	81
MSDZ062	8080	17	4.3	0.35	0.3	0.09	33.115	0.777	672	52
MSDZ063	9890	67	28.7	0.67	1.1	0.14	32.426	1.695	856	70
MSDZ064	12,010	186	10.9	1.8	1.8	0.06	29.728	0.974	754	60
MSDZ065	9780	245	13.3	1.29	1.6	0.16	18.178	1.198	773	68
MSDZ066	10,220	304	36	1.26	1.6	0.15	14.898	1.245	882	234
MSDZ067	10,570	103	15.2	2.37	1.5	0.37	33.987	0.647	787	44
MSDZ068	7490	29	5.1	0.88	1.2	0.08	21.039	1.405	686	61
MSDZ069	10,130	399	4.2	1	1.6	0.16	8.393	1.59	670	61
MSDZ070	7850	31	2.4	0.84	1.4	0.17	12.189	1.672	627	73
MSDZ071	10,570	122	5.3	0.88	1.3	0.06	34.542	1.439	690	69
MSDZ072	8680	36	4	1.18	2.3	0.22	9.333	1.963	667	43
MSDZ073	8860	231	12.3	2.42	3	0.18	10.56	1.241	766	65
MSDZ074	7760	63	35.2	5.95	3.6	0.06	11.811	0.602	880	39
MSDZ075	10,260	209	4.7	2.48	4.4	0.21	8.472	1.755	680	72
MSDZ076	6510	51	5	0.5	0.9	0.2	5.54	1.711	685	58
MSDZ077	7590	25	3.5	0.29	0.4	0.14	16.013	1.495	656	65
MSDZ078	7600	21	2.1	0.63	0.7	0.07	22.823	1.116	617	76
MSDZ079	9740	238	5.3	2.67	4.5	0.14	11.513	1.672	690	56
MSDZ080	10,000	99	8.8	0.67	0.7	0.08	36.364	1.02	734	41
MSDZ081	10,430	213	8.1	2.21	2.6	0.14	15.072	1.181	726	68
MSDZ082	9290	38	7.6	1.44	1.3	0.15	5.63	0.869	721	40
MSDZ083	11,030	318	9.2	1.82	2	0.16	19.25	1.084	738	58
MSDZ084	9300	154	2.8	2.8	4.1	0.13	10.852	1.452	639	77
MSDZ085	9140	674	33.2	25.1	19.6	0.11	6.201	0.781	873	42
MSDZ086	9330	261	6	2.12	3.5	0.14	13.64	1.643	700	76
MSDZ087	9130	150	4.3	2.92	2.9	0.09	14.221	0.993	672	56
MSDZ088	8620	34	5.1	1.35	1.2	0.07	46.596	0.88	686	41
MSDZ089	10,930	110	4.8	1.6	1.4	0.11	51.801	0.899	681	40
MSDZ090	9070	100	7	0.52	0.7	0.09	35.43	1.377	713	76
MSDZ091	8460	485	7	2.78	2.8	0.16	7.05	0.99	713	49
MSDZ092	8300	182	5.5	2.44	3.9	0.16	7.431	1.608	693	54
MSDZ093	10,400	78	7.3	0.94	0.8	0.22	57.143	0.861	717	76
MSDZ094	9750	457	4.5	1.78	2.9	0.15	11.861	1.636	676	62
MSDZ095	5980	46	3.4	0.7	0.6	0.14	14.071	0.829	653	50
MSDZ096	7060	49	3.8	0.58	1.2	0.16	9.605	2.086	662	80
MSDZ097	10,890	275	10	2.21	1.5	0.31	18.272	0.656	746	90
MSDZ098	10,040	163	12.7	0.64	1	0.05	21.004	1.608	769	48
MSDZ099	8830	80	6.8	0.75	0.8	0.09	16.598	1.007	711	89
MSDZ100	9080	137	6.7	1.37	1.4	0.11	24.809	1.047	710	43
MSDZ101	9230	30	12	1.08	1.2	0.17	18.76	1.085	763	244
MSDZ102	11,620	132	8.4	0.54	0.8	0.07	45.214	1.549	730	44
MSDZ103	9550	149	10.9	1.06	1.9	0.12	17.884	1.785	754	60
MSDZ104	7330	26	4.2	0.39	0.9	0.15	9.338	2.234	670	78
MSDZ105	8990	230	10.6	0.93	1.5	0.07	19.168	1.627	751	61
MSDZ106	7980	8	3.5	0.33	0.3	0.07	29.446	1.01	656	90
MSDZ107	10,040	273	6.5	1.03	1.7	0.18	12.395	1.627	707	60
MSDZ108	9140	52	29.3	1.19	1.9	0.1	17.116	1.614	858	53
MSDZ109	7320	21	17	0.54	0.9	0.08	18.164	1.698	798	115
MSDZ110	9170	68	1.7	0.24	0.8	0.05	80.439	3.187	824	54
MSDZ111	9460	31	4.6	1.11	1.1	0.07	29.379	0.999	678	61

Table 3. U, Th, and Pb abundance (in ppm), isotopic geochemical data, and U-Pb core ages (in Ma) for the southern Meiganga detrital zircons.

Sample Spot-Number	U	Th	Pb	Th/U	$^{207}Pb/^{206}Pb$	2s%	$^{207}Pb/^{235}U$	2s%	$^{206}Pb/^{238}U$	2s%	6/38–7/35 Rho	$^{207}Pb/^{206}Pb$ (Ma) Age	2s. Abs.	$^{207}Pb/^{235}U$ Age (Ma)	2s. Abs.	$^{206}Pb/^{238}U$ Age (Ma)	2s. Abs.	% Discordance (6/38–7/35)	% Discordance (6/38–7/6)
MSDZ001	522	154	122	0.296	0.12425	1.0287	4.889	2.1541	0.2869	1.8925	0.88	2018	18	1800	39	1626	31	9.7	19.4
MSDZ002	145	79	119	0.537	0.26727	1.0095	21.49	2.0761	0.5848	1.8141	0.87	3290	16	3160	66	2968	54	6.1	9.8
MSDZ003	69	48	74	0.704	0.22325	1.0507	17.77	2.0178	0.5797	1.7226	0.85	3004	17	2977	60	2948	51	1	1.9
MSDZ004	259	341	407	1.315	0.17496	1.0996	10.468	2.1677	0.4356	1.8681	0.86	2605	18	2477	54	2330	44	5.9	10.6
MSDZ005	124	177	498	1.431	0.315	3.6324	24.7	4.1461	0.5676	1.9988	0.48	3531	56	3283	136	2902	58	11.6	17.8
MSDZ006	598	165	114	0.275	0.15845	1.0314	5.201	2.5306	0.2399	2.3109	0.91	2439	17	1852	47	1386	32	25.2	43.2
MSDZ007	54	16	23	0.287	0.21296	1.065	15.34	2.0274	0.5269	1.7252	0.85	2928	17	2836	58	2728	47	3.8	6.8
MSDZ008	488	268	259	0.55	0.13435	1.1417	5.984	2.0884	0.3259	1.7487	0.84	2155	20	1973	41	1818	32	7.9	15.6
MSDZ009	66	70	108	1.046	0.221	1.0243	17.08	1.9976	0.5669	1.715	0.86	2988	16	2939	59	2895	50	1.5	3.1
MSDZ010	495	230	207	0.462	0.13476	1.0858	5.779	2.1565	0.3142	1.8632	0.86	2161	19	1943	42	1761	33	9.4	18.5
MSDZ011	338	217	174	0.632	0.1226	1.3435	4.43	2.2949	0.2633	1.8605	0.81	1993	24	1719	39	1507	28	12.3	24.4
MSDZ012	105	42	55	0.403	0.20116	1.0216	13.09	2.0777	0.4736	1.8092	0.87	2836	17	2685	56	2502	45	6.8	11.8
MSDZ013	338	299	323	0.88	0.13567	1.0905	6.657	2.0879	0.3585	1.7805	0.85	2174	19	2067	43	1975	35	4.4	9.1
MSDZ014	509	116	109	0.228	0.13695	1.1887	6.03	2.2048	0.3183	1.857	0.84	2189	21	1980	44	1781	33	10.1	18.6
MSDZ015	954	123	46	0.128	0.08105	1.2155	1.2248	2.1535	0.10972	1.7777	0.83	1224	24	812	17	671	12	17.3	45.2
MSDZ016	27	12	19	0.451	0.22252	1.0873	17.52	2.1095	0.5705	1.8077	0.86	2999	17	2963	63	2910	53	1.8	3
MSDZ017	125	217	238	1.715	0.16046	1.0369	8.15	2.2115	0.3659	1.9533	0.88	2461	18	2247	50	2010	39	10.5	18.3
MSDZ018	77	44	67	0.568	0.22195	1.0271	16.69	2.0589	0.5443	1.7844	0.87	2995	17	2920	60	2801	50	4.1	6.5
MSDZ019	79	22	35	0.279	0.21649	1.0693	16.41	2.0471	0.5445	1.7456	0.85	2955	17	2901	59	2802	49	3.4	5.2
MSDZ020	47	38	62	0.799	0.21889	1.0345	17.29	2.014	0.567	1.728	0.86	2973	17	2951	59	2895	50	1.9	2.6
MSDZ021	189	87	123	0.46	0.19979	1.063	12.675	2.0103	0.4554	1.7063	0.85	2824	17	2656	53	2419	41	8.9	14.4
MSDZ022	219	264	365	1.203	0.17656	1.1383	10.966	2.1316	0.4461	1.8022	0.85	2620	19	2520	54	2380	43	5.6	9.2
MSDZ023	192	253	270	1.319	0.13305	1.0486	6.229	2.0321	0.3355	1.7407	0.86	2139	18	2008	41	1865	32	7.1	12.8
MSDZ024	313	161	168	0.51	0.1345	1.3402	5.942	2.1893	0.3177	1.7312	0.79	2156	23	1967	43	1778	31	9.6	17.5
MSDZ025	734	269	112	0.365	0.08579	1.1816	1.445	2.1	0,.1217	1.7361	0.83	1333	23	908	19	740	13	18.5	44.5
MSDZ026	229	263	374	1.136	0.17876	1.1196	11.09	2.158	0.4464	1.8449	0.85	2641	19	2530	55	2379	44	6	9.9
MSDZ027	238	155	166	0.653	0.13304	1.1592	6.056	2.1298	0.327	1.7867	0.84	2138	20	1984	42	1824	33	8	14.7
MSDZ028	166	155	208	0.923	0.17506	1.0553	10.65	2.0759	0.4389	1.7877	0.86	2607	18	2493	52	2345	42	5.9	10
MSDZ029	38	22	38	0.585	0.21003	1.0526	15.66	2.186	0.5409	1.9159	0.88	2906	17	2855	62	2791	53	2.2	3.9
MSDZ030	125	70	84	0.553	0.13283	1.0466	6.889	2.1274	0.3751	1.8522	0.87	2136	18	2097	45	2053	38	2.1	3.9
MSDZ031	32	9	14	0.277	0.1965	1.122	13.7	2.2204	0.5028	1.916	0.86	2797	18	2729	61	2625	50	3.8	6.1
MSDZ032	240	78	112	0.321	0.2201	1.139	14.35	2.4437	0.4745	2.1621	0.88	2981	18	2772	68	2502	54	9.7	16.1
MSDZ033	95	71	74	0.748	0.12894	1.067	5.737	2.4103	0.3235	2.1612	0.9	2083	19	1938	47	1806	39	6.8	13.3
MSDZ034	48	19	32	0.383	0.22028	1.0578	17.57	2.4692	0.5788	2.2311	0.9	2983	17	2965	73	2943	66	0.7	1.3
MSDZ035	330	466	164	1.393	0.06227	1.0503	0.9296	2.0932	0.1086	1.8106	0.86	683	22	667	14	664	12	0.4	2.8
MSDZ036	449	160	147	0.35	0.12971	1.122	5.145	2.1521	0.2884	1.8365	0.85	2094	20	1843	40	1635	30	11.3	21.9
MSDZ037	150	298	334	1.976	0.13175	1.0836	6.657	2.1093	0.3666	1.8097	0.86	2123	19	2067	44	2013	36	2.6	5.2
MSDZ038	32	16	24	0.5	0.19623	1.0583	13.83	2.0647	0.5109	1.7728	0.86	2795	17	2738	57	2660	47	2.9	4.8

Table 3. *Cont.*

Sample Spot-Number	U	Th	Pb	Th/U	^{207}Pb/^{206}Pb	2s%	^{207}Pb/^{235}U	2s%	^{206}Pb/^{238}U	2s%	6/38–7/35 Rho	^{207}Pb/^{206}Pb (Ma) Age	2s. Abs.	^{207}Pb/^{235}U Age (Ma)	2s. Abs.	^{206}Pb/^{238}U Age (Ma)	2s. Abs.	% Discordance (6/38–7/35)	% Discordance (6/38–7/6)
MSDZ039	237	266	339	1.122	0.17017	1.039	9.84	2.2355	0.4205	1.9794	0.89	2559	17	2420	54	2262	45	6.5	11.6
MSDZ040	76	13	20	0.172	0.2141	1.1699	15.57	2.3122	0.5291	1.9944	0.86	2937	19	2855	66	2737	55	4.1	6.8
MSDZ041	306	334	346	1.088	0.13399	1.0674	6.614	2.144	0.3589	1.8594	0.87	2151	19	2062	44	1977	37	4.1	8.1
MSDZ042	137	334	373	2.381	0.13342	1.044	6.981	2.1077	0.3819	1.831	0.87	2143	18	2109	44	2085	38	1.1	2.7
MSDZ043	130	97	34	0.741	0.06126	1.1855	0.8834	2.1325	0.1049	1.7726	0.83	648	25	643	14	643	11	0	0.8
MSDZ044	433	91	87	0.207	0.13238	1.1884	5.563	2.2081	0.3051	1.861	0.84	2129	21	1910	42	1716	32	10.2	19.4
MSDZ045	69	45	63	0.647	0.19738	1.056	13.14	2.1316	0.4829	1.8516	0.87	2805	17	2690	57	2543	47	5.4	9.3
MSDZ046	396	26	27	0.065	0.13906	1.1228	6.707	2.3098	0.3494	2.0186	0.87	2215	19	2073	48	1931	39	6.9	12.8
MSDZ047	204	180	188	0.873	0.13205	1.0892	6.139	2.1421	0.3378	1.8445	0.86	2125	19	1997	43	1876	35	6	11.7
MSDZ048	146	203	270	1.37	0.17176	1.1007	10.69	2.1434	0.4521	1.8391	0.86	2575	18	2497	54	2404	44	3.7	6.6
MSDZ049	160	145	140	0.897	0.12653	1.1206	5.585	2.0822	0,.3191	1.7549	0.84	2050	20	1913	40	1785	31	6.7	12.9
MSDZ050	112	36	59	0.321	0.22315	1.0536	17.16	2.1308	0.5574	1.8521	0.87	3004	17	2944	63	2859	53	2.9	4.8
MSDZ051	297	100	109	0.333	0.13008	1.1179	6.321	2.2149	0.3534	1.9121	0.86	2099	20	2021	45	1951	37	3.5	7
MSDZ052	360	347	374	0.956	0.13702	1.14	6.766	2.1137	0.359	1.78	0.84	2190	20	2082	44	1977	35	5	97
MSDZ053	294	122	117	0.405	0.1303	1.0854	5.516	2.3289	0.3081	2.0605	0.88	2102	19	1902	44	1731	36	9	17.6
MSDZ054	236	91	131	0.381	0.2234	1.1147	15.49	2.0905	0.5043	1.7686	0.85	3005	18	2846	59	2632	47	7.5	12.4
MSDZ055	93	153	465	1.621	0.3421	1.4946	28.27	2.2929	0.6021	1.7389	0.76	3671	23	3428	79	3038	53	11.4	17.2
MSDZ056	191	363	484	1.887	0.17582	1.1157	11.461	2.1782	0.4745	1.8708	0.86	2614	19	2561	56	2503	47	2.3	4.2
MSDZ057	44	20	29	0.464	0.19934	1.0387	13.85	2.5014	0.5068	2.2755	0.91	2821	17	2738	68	2642	60	3.5	6.3
MSDZ058	169	208	265	1.222	0.16976	1.0316	10.47	2.2061	0.4485	1.9501	0.88	2555	17	2476	55	2388	47	3.6	6.5
MSDZ059	151	138	143	0.907	0.13006	1.0462	6.428	2.1954	0.3613	1.9301	0.88	2099	18	2037	45	1988	38	2.4	5.3
MSDZ060	44	19	31	0.438	0.2195	1.0496	17.87	2.1974	0.5925	1.9305	0.88	2978	17	2982	66	2999	58	−0.6	−0.7
MSDZ061	55	17	21	0.313	0.18958	1.0624	11.65	2.2321	0.4484	1.9631	0.88	2738	17	2578	58	2391	47	7.3	12.7
MSDZ062	38	17	27	0.448	0.21604	1.0484	17.2	2.1184	0.5823	1.8408	0.87	2951	17	2946	62	2958	54	−0.4	−0.2
MSDZ063	224	67	88	0.301	0.19233	1.066	12.28	2.2693	0.4645	2.0034	0.88	2763	17	2625	60	2459	49	6.3	11
MSDZ064	339	186	164	0.545	0.12804	1.0388	5.534	2.2585	0.3143	2.0054	0.89	2071	18	1906	43	1762	35	7.5	14.9
MSDZ065	229	245	240	1.058	0.13116	1.1061	6.202	2.2089	0.3439	1.912	0.87	2113	19	2004	44	1905	36	5	9.9
MSDZ066	277	304	248	1.103	0.12381	1.0218	5.26	2.1466	0.3094	1.8878	0.88	2012	18	1862	40	1738	33	6.7	13.6
MSDZ067	576	103	63	0.179	0.1355	1.4918	3.806	2.3417	0.2035	1.805	0.77	2169	26	1593	37	1194	22	25	45
MSDZ068	62	29	41	0.463	0.18511	1.0242	12.67	2.0947	0.4986	1.8272	0.87	2699	17	2656	56	2607	48	1.9	3.4
MSDZ069	140	399	527	2.817	0.16994	1.0529	11.05	2.1488	0.4723	1.8731	0.87	2557	18	2528	54	2493	47	1.4	2.5
MSDZ070	71	31	43	0.43	0.19918	1.0429	13.31	2.3448	0.4852	2.1001	0.9	2820	17	2703	63	2549	54	5.7	9.6
MSDZ071	240	122	121	0.505	0.13048	1.0975	6.104	2.184	0.3391	1.8882	0.86	2104	19	1990	43	1882	36	5.4	10.6
MSDZ072	134	36	53	0.256	0.21533	1.0968	15.99	2.1918	0.5391	1.8976	0.87	2947	18	2878	63	2779	53	3.4	5.7
MSDZ073	97	231	299	2.331	0.1689	1.0517	10.58	2.1776	0.4531	1.9069	0.88	2547	18	2487	54	2409	46	3.1	5.4
MSDZ074	182	63	21	0.341	0.065	1.1662	0.9	2.1599	0.1008	1.818	0.84	774	25	652	14	619	11	5	20

Table 3. *Cont.*

Sample Spot-Number	U	Th	Pb	Th/U	$^{207}Pb/^{206}Pb$	2s%	$^{207}Pb/^{235}U$	2s%	$^{206}Pb/^{238}U$	2s%	6/38–7/35 Rho	$^{207}Pb/^{206}Pb$ (Ma) Age	2s. Abs.	$^{207}Pb/^{235}U$ Age (Ma)	2s. Abs.	$^{206}Pb/^{238}U$ Age (Ma)	2s. Abs.	% Discordance (6/38–7/35)	% Discordance (6/38–7/6)
MSDZ075	161	209	282	1.274	0.17388	1.0868	11.62	2.2744	0.4847	1.998	0.88	2595	18	2574	59	2547	51	1	1.9
MSDZ076	93	51	79	0.535	0.21857	1.037	17.28	2.1931	0.5721	1.9325	0.88	2970	17	2950	65	2916	56	1.2	1.8
MSDZ077	96	25	31	0.257	0.20631	1.0225	13.89	2.5455	0.4896	2.3311	0.92	2877	17	2742	70	2569	60	6.3	10.7
MSDZ078	43	21	23	0.5	0.14038	1.1174	6.704	2.071	0.3463	1.7436	0.84	2232	19	2073	43	1917	33	7.5	14.1
MSDZ079	198	238	297	1.189	0.17122	1.0635	10.3	2.3104	0.4364	2.051	0.89	2569	18	2461	57	2334	48	5.2	9.2
MSDZ080	183	99	103	0.525	0.1309	1.0705	6.319	2.2667	0.351	1.998	0.88	2110	19	2021	46	1939	39	4	8.1
MSDZ081	338	213	212	0.618	0.13361	1.1431	6.257	2.3372	0.3404	2.0386	0.87	2146	20	2014	47	1888	38	6.2	12
MSDZ082	265	38	48	0.142	0.1964	1.2583	11.22	2.3151	0.4171	1.9433	0.84	2796	21	2543	59	2247	44	11.6	19.6
MSDZ083	464	318	316	0.676	0.1366	1.2139	6.22	2.4767	0.3312	2.1588	0.87	2184	21	2007	50	1844	40	8.1	15.6
MSDZ084	137	154	211	1.099	0.17027	1.0564	10.781	2.1134	0.4612	1.8304	0.87	2560	18	2504	53	2445	45	2.4	4.5
MSDZ085	461	674	219	1.441	0.06096	1.1145	0.8321	2.1662	0.0996	1.8575	0.86	637	24	615	13	612	11	0.4	3.9
MSDZ086	100	261	369	2.564	0.17089	1.0598	11.4	2.1486	0.4865	1.869	0.87	2566	18	2556	55	2555	48	0	0.4
MSDZ087	94	150	216	1.55	0.17263	1.0727	11.48	2.1035	0.4852	1.8094	0.86	2583	18	2563	54	2549	46	0.5	1.3
MSDZ088	161	34	47	0.205	0.1992	1.2223	13.16	2.4488	0.4807	2.122	0.87	2819	20	2693	66	2530	54	6.1	10.3
MSDZ089	299	110	126	0.36	0.163	1.2791	8.47	2.5914	0.378	2.2538	0.87	2486	22	2282	59	2066	47	9.5	16.9
MSDZ090	311	100	109	0.319	0.1353	1.2435	6.19	2.6886	0.3339	2.3838	0.89	2168	22	2001	54	1856	44	7.2	14.4
MSDZ091	549	485	570	0.88	0.1463	1.5855	6.59	3.149	0.3272	2.7207	0.86	2302	27	2057	65	1824	50	11.3	20.8
MSDZ092	141	182	267	1.264	0.17642	1.1076	11.81	2.3478	0.4872	2.0702	0.88	2619	18	2589	61	2558	53	1.2	2.3
MSDZ093	431	78	86	0.175	0.1648	1.3121	7.959	2.5126	0.3508	2.1428	0.85	2504	22	2226	56	1942	42	12.8	22.4
MSDZ094	240	457	509	1.876	0.13638	1.2104	6.991	2.4474	0.371	2.1271	0.87	2181	21	2110	52	2034	43	3.6	6.7
MSDZ095	101	46	77	0.442	0.2282	1.1967	17.74	2.5354	0.5638	2.2352	0.88	3041	19	2974	75	2881	64	3.1	5.3
MSDZ096	162	49	70	0.292	0.1981	1.1961	12.82	2.3474	0.4705	2.0198	0.86	2810	20	2668	63	2485	50	6.9	11.6
MSDZ097	516	275	248	0.526	0.1349	1.3888	5.735	2.498	0.3098	2.0764	0.83	2164	24	1936	48	1739	36	10.2	19.6
MSDZ098	183	163	155	0.874	0.12897	1.0566	6.096	2.3265	0.3415	2.0728	0.89	2084	19	1989	46	1893	39	4.8	9.2
MSDZ099	70	80	93	1.119	0.14679	1.0909	6.476	2.1416	0.3171	1.8429	0.86	2309	19	2042	44	1776	33	13	23.1
MSDZ100	119	137	134	1.133	0.12738	1.0554	5.962	2.1	0.338	1.8155	0.86	2062	19	1971	41	1877	34	4.8	9
MSDZ101	103	30	32	0.289	0.15633	1.0461	7.902	2.0903	0.3666	1.8097	0.87	2416	18	2220	46	2013	36	9.3	16.7
MSDZ102	379	132	131	0.345	0.13019	1.1109	5.72	2.2848	0.3182	1.9965	0.87	2100	20	1936	44	1780	36	8	15.2
MSDZ103	184	149	157	0.804	0.12858	1.0218	6.667	2.249	0.3732	2.0035	0.89	2079	18	2068	47	2044	41	1.2	1.7
MSDZ104	84	26	34	0.314	0.17747	1.0574	10.85	2.2772	0.4398	2.0168	0.89	2629	18	2511	57	2353	47	6.3	10.5
MSDZ105	149	230	316	1.538	0.18392	1.0681	12.86	2.1207	0.5042	1.8321	0.86	2688	18	2669	57	2632	48	1.4	2.1
MSDZ106	25	8	8	0.316	0.1316	1.3033	6.12	2.7694	0.3357	2.4436	0.88	2121	23	1994	55	1865	46	6.5	12.1
MSDZ107	244	273	275	1.05	0.12861	1.0786	6.128	2.1541	0.3447	1.8645	0.87	2079	19	1995	43	1909	36	4.3	8.2
MSDZ108	81	52	72	0.63	0.17535	1.0746	12.35	2.8957	0.509	2.6889	0.93	2609	18	2636	76	2649	71	−0.5	−1.5
MSDZ109	33	21	25	0.624	0.1671	1.3438	9.35	2.3794	0.4041	1.9636	0.83	2528	23	2375	57	2188	43	7.9	13.4
MSDZ110	100	68	70	0.67	0.12757	1.037	6.272	2.1746	0.3538	1.9115	0.88	2065	18	2014	44	1952	37	3.1	5.5
MSDZ111	92	31	40	0.332	0.16737	1.0728	10.878	2.0171	0.4681	1.7082	0.85	2531	18	2513	51	2475	42	1.5	2.2

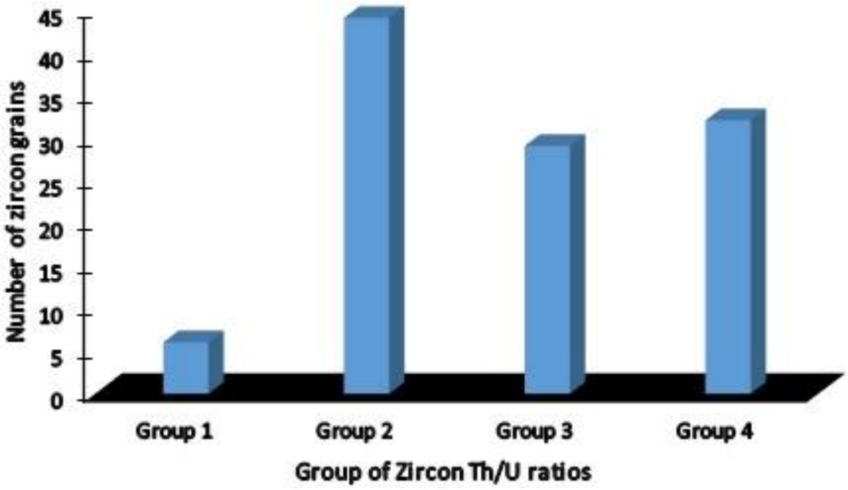

Figure 3. Number of zircon grains in various classified Th/U ratio's groups (group 1: Th/U < 0.2, group 2: Th/U [0.2–0.5], group 3: Th/U [0.5–1.0], and group 4: Th/U > 1.0).

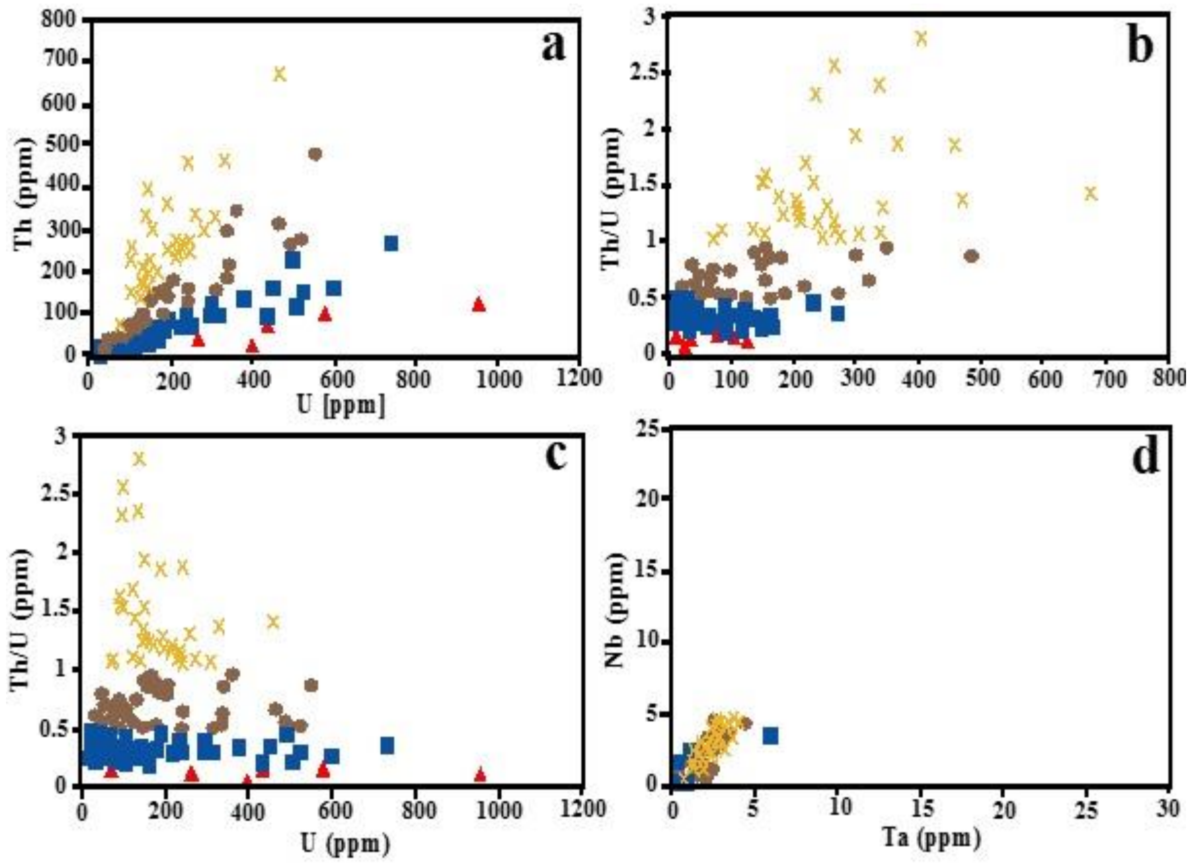

Figure 4. Geochemical correction of various elements/ratios within the southern Meiganga detrital zircons: (**a**) Th versus U; (**b**) Th/U versus Th; (**c**) Th/U versus U; (**d**) Nb versus Ta (red triangles represent zircon with Th/U < 0.2; blue squares represent zircon with Th/U ratios [0.2 to 0.5]; brown circles represent zircons with Th/U ratios [>0.5 to 0.956]; and yellow stars represent zircons with Th/U > 1.0).

The Ti, Ta, Nb, and Sr contents (<48 ppm) are generally low. This indicates low degrees of substitution of these elements within the crystal structure of zircon. Within these element suites, Ti contents (2 to 256 ppm) are globally less than 12 ppm; with the highest value (256 ppm) being that of MSDZ055. Low Ti-zircons generally have low Th and U, which clearly differentiate them from others. The calculated Ti-zircon temperatures

(617 to 1180 °C) (Table 2) are mainly more than 700 °C, with the predominance of zircons whose temperatures ranging from 700–717 °C, 680–694 °C, and 720–728 °C. The highest temperatures are that of MSDZ008 and MSDZ055. The Ta and Nb abundances are generally very close (Figure 4d), and vary from 0.2 to 25.1 ppm and 0.3 to 19.6 ppm, respectively. The highest Ta (25.1 ppm) and Nb (19.6 ppm) values were found in MSDZ085, which also has the highest Th (674 ppm) and relatively high Y (1474 ppm), U (461 ppm), and Ti (33.2 ppm) contents. The Nb/Ta ratios vary from 0.6 to 3.4, with the highest values generally being for zircons with Hf contents (<9000 ppm) and Y contents (>361 to 931 ppm).

4.1.3. Rare Earth Elements (REE)

The REE abundances (Table 4) are variable with the values of total light rare earth elements (LREE: La-Pr) being generally less than those of middle rare earth elements (MREE: Nd-Gd) and heavy rare earth elements (HREE: Tb-Lu). The total rare elements (∑REE) range from 43 to 1030 ppm, with most values being less 400 ppm. Lowest ∑REE contents are that of MSDZ030 (43 ppm), MSDZ046 (98 ppm), and MSDZ059 (79 ppm), of which the normalized patterns (Figure 5a–g) are different from others.

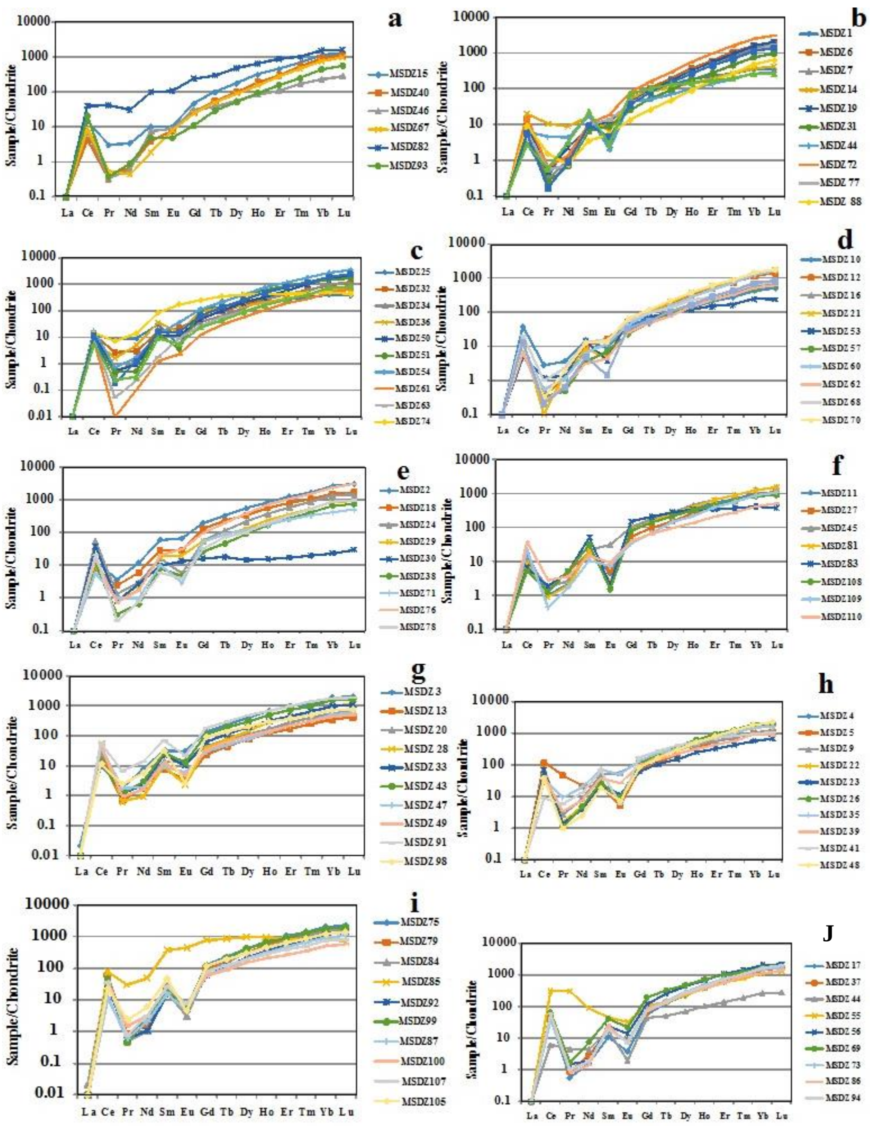

Figure 5. REE patterns for southern Meiganga zircons normalized to [69], chondrite values versus element (La–Lu) diagrams ((**a**) zircon with Th/U < 0.2; (**b**–**d**) zircon with Th/U [0.2 to 0.5]; (**e**–**g**) zircon with Th/U [>0.5 to 1.0]; (**h**–**j**) zircon with Th/U > 1.0).

Table 4. Rare earth element abundance (in ppm) in the southern Meiganga detrital zircons. REE (rare earth elements).

Sample Spot-Name	La	Ce	Pr	Nd	Sm	Eu	Gd	Tb	Dy	Ho	Er	Tm	Yb	Lu	∑REE	Gd/Yb	Lu/Hf	Sm/La_N	Ce/Ce*	Eu/Eu*
MSDZ001	bdl	2	0	1.5	3.2	0.13	14	3.6	32	10	36	6	57	9	173	0.246	0.001	-	-	0.06
MSDZ002	bdl	9	0.3	5.7	9.1	3.87	40	12.1	139	47	210	43	432	78	1029	0.092	0.01	-	-	0.62
MSDZ003	0.01	6	0.2	3.6	4.9	1.73	27	8.5	102	37	158	30	310	51	741	0.087	0.007	1569.299	50.443	0.46
MSDZ004	bdl	30	0.1	2.1	3.3	0.49	20	7.1	82	29	132	28	264	47	645	0.075	0.005	-	-	0.19
MSDZ005	bdl	76	4.4	10.3	3.1	0.3	14	4.3	53	20	90	19	174	29	497	0.082	0.003	-	-	0.14
MSDZ006	bdl	9	0	0.5	1	0.71	8	3.8	48	20	101	26	257	51	526	0.032	0.006	-	-	0.77
MSDZ007	bdl	3	0	0.4	1.1	0.67	8	3.3	44	18	87	21	226	45	457	0.036	0.007	-	-	0.68
MSDZ008	bdl	4	0.1	1.5	3.4	0.14	16	5.2	52	17	68	13	116	17	313	0.138	0.002	-	-	0.06
MSDZ009	bdl	21	0.2	3.9	7.4	3.26	27	7.1	77	25	100	19	171	30	492	0.158	0.004	-	-	0.71
MSDZ010	bdl	23	0.3	1.7	2.2	0.52	8	2.3	24	8	34	7	67	13	191	0.121	0.001	-	-	0.37
MSDZ011	bdl	11	0.1	1	3.4	0.26	17	5.8	62	22	87	17	172	28	426	0.101	0.003	-	-	0.1
MSDZ012	bdl	7	0	0.6	1.5	0.95	9	3.5	41	19	85	19	183	36	404	0.048	0.005	-	-	0.8
MSDZ013	bdl	13	0.1	0.8	1.2	0.19	5	1.6	20	7	27	6	57	11	149	0.083	0.001	-	-	0.24
MSDZ014	bdl	13	1	4.2	2.6	0.37	12	3.2	27	8	32	7	64	11	185	0.181	0.001	-	-	0.21
MSDZ015	bdl	9	0.3	1.6	1.5	0.57	10	3.7	45	17	74	17	183	32	394	0.052	0.003	-	-	0.46
MSDZ016	bdl	3	0.1	0.6	1	0.68	6	2.2	26	10	43	10	101	17	220	0.059	0.003	-	-	0.85
MSDZ017	bdl	29	0.1	0.8	1.7	0.22	12	4.7	56	22	99	23	245	40	533	0.047	0.004	-	-	0.15
MSDZ018	bdl	5	0.2	2.8	4.5	1.59	28	8.6	86	31	130	28	259	43	627	0.106	0.006	-	-	0.44
MSDZ019	bdl	6	0	1.1	1.4	0.74	8	3.2	43	18	94	23	261	52	512	0.032	0.007	-	-	0.67
MSDZ020	bdl	19	0.1	1.2	2.1	0.84	9	2.7	28	10	45	10	96	16	239	0.092	0.002	-	-	0.6
MSDZ021	bdl	9	0	0.8	1.3	0.28	10	4	49	21	97	22	232	45	491	0.043	0.005	-	-	0.24
MSDZ022	bdl	47	0.1	2.2	3.9	0.55	19	6.8	71	27	115	26	250	44	613	0.076	0.005	-	-	0.2
MSDZ023	bdl	43	0.1	1.8	3.7	0.64	13	3.9	39	14	54	11	94	17	296	0.132	0.002	-	-	0.29
MSDZ024	bdl	35	0.1	1.3	2.4	0.32	11	4.2	53	21	96	22	218	36	499	0.051	0.004	-	-	0.19
MSDZ025	bdl	7	0.8	4.2	4.7	0.29	22	5.4	50	13	42	8	66	10	233	0.329	0.001	-	-	0.09
MSDZ026	bdl	26	0.1	2.3	4.1	0.54	24	8.3	98	35	157	32	321	53	761	0.075	0.006	-	-	0.17
MSDZ027	bdl	5	0.2	2.2	3	0.31	11	3.5	38	14	68	14	149	28	337	0.072	0.003	-	-	0.17
MSDZ028	bdl	34	0.1	0.4	1.5	0.13	8	2.8	37	16	69	16	164	29	379	0.051	0.003	-	-	0.12
MSDZ029	bdl	6	0.1	0.8	2.7	1.14	11	3	32	13	56	13	138	23	300	0.081	0.003	-	-	0.63
MSDZ030	bdl	24	0.1	1.2	1.5	0.77	3	0.6	4	1	3	0	4	1	43	0.836	9.628	-	-	1.09
MSDZ031	bdl	3	0	0.3	1	0.5	5	2	23	10	45	11	123	24	248	0.042	0.003\	-	-	0.65
MSDZ032	bdl	8	0.3	1.4	2.6	1.32	11	3.4	43	16	71	15	157	28	358	0.073	0.004	-	-	0.75
MSDZ033	bdl	29	0.1	1.1	3.3	0.58	13	4.2	48	18	75	17	158	28	394	0.082	0.003	-	-	0.27

Table 4. *Cont.*

Sample Spot-Name	La	Ce	Pr	Nd	Sm	Eu	Gd	Tb	Dy	Ho	Er	Tm	Yb	Lu	∑REE	Gd/Yb	Lu/Hf	Sm/La_N	Ce/Ce*	Eu/Eu*
MSDZ034	bdl	8	0	0.7	1.6	0.6	8	2.4	31	14	66	14	169	27	343	0.045	0.003	-	-	0.53
MSDZ035	bdl	22	0.9	9.4	11.2	3.02	29	9	81	27	123	26	254	41	636	0.113	0.004	-	-	0.51
MSDZ036	bdl	5	0.2	2.3	5.4	0.9	19	4.5	38	11	47	10	95	17	255	0.195	0.002	-	-	0.27
MSDZ037	bdl	29	0.1	1.3	2.6	0.48	13	5.1	61	23	110	23	234	42	545	0.057	0.004	-	-	0.25
MSDZ038	bdl	7	0	0.3	1.2	0.26	5	1.7	23	9	43	10	110	19	230	0.05	0.002	-	-	0.32
MSDZ039	bdl	27	0.3	3.5	5.7	1.49	20	5.3	57	18	71	15	149	21	394	0.136	0.003	-	-	0.42
MSDZ040	bdl	3	0	0.3	0.6	0.43	5	2	25	11	48	14	154	29	291	0.035	0.003	-	-	0.73
MSDZ041	bdl	6	0.6	6.1	10	0.34	35	9.9	101	31	114	21	162	27	523	0.217	0.003	-	-	0.06
MSDZ042	bdl	30	0.1	1.1	2.9	0.57	15	4.8	56	20	88	19	184	32	454	0.08	0.003	-	-	0.27
MSDZ043	bdl	8	0.1	1.4	4.3	0.75	24	7.5	76	29	121	26	270	44	612	0.088	0.005	-	-	0.23
MSDZ044	bdl	4	0.4	2.1	2.7	0.11	9	1.9	18	6	23	5	45	7	123	0.2	0.001	-	-	0.07
MSDZ045	bdl	7	0.2	1.2	3.3	1.73	21	6.4	69	25	103	22	207	38	504	0.1	0.005	-	-	0.64
MSDZ046	bdl	5	0	0.3	1.1	0.51	6	1.4	14	5	17	4	37	7	98	0.163	0.001	-	-	0.59
MSDZ047	bdl	26	0.2	0.9	1.4	0.35	6	1.8	19	7	35	8	83	15	205	0.074	0.002	-	-	0.36
MSDZ048	bdl	24	0.1	1.2	2.8	0.42	17	6.3	76	30	138	31	315	58	699	0.054	0.006	-	-	0.19
MSDZ049	bdl	32	0.1	0.7	2	0.27	7	2.3	25	8	35	8	70	13	203	0.097	0.001	-	-	0.22
MSDZ050	bdl	7	0.1	0.4	1.7	0.65	10	3.7	50	18	95	25	250	50	511	0.038	0.006	-	-	0.49
MSDZ051	bdl	5	0	0.2	2.1	0.21	21	8.2	99	35	146	29	253	43	640	0.081	0.004	-	-	0.1
MSDZ052	bdl	32	0.1	0.6	1.8	0.61	13	4.5	56	22	95	20	208	38	492	0.064	0.004	-	-	0.38
MSDZ053	bdl	3	0.1	0.6	2.1	0.22	11	2.7	25	7	24	4	40	6	126	0.274	0.001	-	-	0.14
MSDZ054	bdl	11	0.1	0.8	2	2.11	24	8.3	103	43	199	46	461	88	989	0.052	0.011	-	-	0.94
MSDZ055	bdl	187	28.8	41.3	6.7	1.88	21	5.1	56	20	94	19	184	32	698	0.115	0.003	-	-	0.48
MSDZ056	bdl	30	0.1	0.9	3.5	0.8	25	9.4	107	37	172	37	339	54	815	0.073	0.005	-	-	0.26
MSDZ057	bdl	5	0	0.2	0.5	0.4	5	1.8	23	8	37	9	79	15	184	0.058	0.002	-	-	0.78
MSDZ058	bdl	30	0.1	1.1	2.5	0.49	24	10.2	113	41	174	38	348	60	841	0.068	0.006	-	-	0.19
MSDZ059	bdl	53	0.2	1.6	2	1.13	6	1	6	1	3	1	3	0	79	2.37	4.055	-	-	0.97
MSDZ060	bdl	6	0.1	0.5	1	0.69	9	3.5	39	16	78	19	210	41	422	0.04	0.005	-	-	0.73
MSDZ061	bdl	5	bdl	0	0.2	0.13	3	1.1	15	6	32	7	76	16	161	0.033	0.002	-	-	0.58
MSDZ062	bdl	4	0	0.3	0.5	0.25	5	1.8	19	8	37	8	84	16	185	0.062	0.002	-	-	0.49
MSDZ063	bdl	6	0	0.1	0.3	0.53	5	2.1	24	9	43	11	109	20	230	0.05	0.002	-	-	1.33
MSDZ064	bdl	3	0.1	1.5	3.2	0.06	22	5.1	46	12	40	7	47	7	194	0.463	0.001	-	-	0.02
MSDZ065	bdl	15	0.1	1.8	3.1	0.33	18	5.7	56	19	74	15	136	23	367	0.134	0.002	-	-	0.13
MSDZ066	bdl	6	0.2	1.8	4	1.71	21	6.8	69	21	88	17	150	27	413	0.14	0.003	-	-	0.57

Table 4. *Cont.*

Sample Spot-Name	La	Ce	Pr	Nd	Sm	Eu	Gd	Tb	Dy	Ho	Er	Tm	Yb	Lu	∑REE	Gd/Yb	Lu/Hf	Sm/La_N	Ce/Ce*	Eu/Eu*
MSDZ067	bdl	6	0.1	0.2	0.3	0.47	5	1.9	23	9	46	12	126	25	254	0.039	0.002	-	-	1.21
MSDZ068	bdl	13	0.1	1.1	2.1	0.89	11	3.5	34	13	46	11	106	19	259	0.105	0.003	-	-	0.57
MSDZ069	bdl	41	0.2	3.4	6.1	1.23	39	12	118	39	162	31	274	46	773	0.142	0.005	-	-	0.24
MSDZ070	bdl	7	0	0.9	1.9	0.79	13	4.5	55	21	101	23	246	45	519	0.053	0.006	-	-	0.48
MSDZ071	bdl	3	0.1	0.5	1.5	0.17	11	3.2	29	10	41	8	68	12	188	0.155	0.001	-	-	0.13
MSDZ072	bdl	10	0.1	0.7	1.6	1.09	16	5.8	75	32	161	40	412	77	832	0.038	0.009	-	-	0.65
MSDZ073	bdl	23	0.1	0.8	3.4	0.45	17	5.8	73	27	126	25	255	43	599	0.066	0.005	-	-	0.18
MSDZ074	bdl	9	0.7	6.4	12.7	10.15	51	12.9	101	24	73	11	83	11	406	0.609	0.001	-	-	1.22
MSDZ075	bdl	32	0.1	1.2	4	0.3	25	8.4	106	38	173	36	339	57	820	0.074	0.006	-	-	0.09
MSDZ076	bdl	10	0.1	0.8	3.1	1.79	20	7.4	94	39	178	39	401	77	870	0.049	0.012	-	-	0.7
MSDZ077	bdl	4	0.1	0.3	1.4	0.77	8	3	38	15	77	17	181	41	387	0.043	0.005	-	-	0.71
MSDZ078	bdl	13	0	0.4	0.9	0.23	7	2.7	25	11	53	13	142	24	292	0.047	0.003	-	-	0.29
MSDZ079	bdl	37	0.1	0.7	3.1	0.34	19	6.4	80	30	124	26	244	45	615	0.08	0.005	-	-	0.14
MSDZ080	bdl	3	0.1	0.8	2.4	0.09	12	3.2	30	8	34	7	65	11	177	0.188	0.001	-	-	0.05
MSDZ081	bdl	6	0.1	0.9	3.2	0.14	17	5.5	66	23	105	22	202	39	488	0.083	0.004	-	-	0.06
MSDZ082	bdl	25	4	14.3	15	6.26	49	11	120	36	142	25	247	40	735	0.198	0.004	-	-	0.7
MSDZ083	bdl	4	0.2	2.4	7.6	0.11	30	7.5	71	19	56	10	69	9	286	0.443	0.001	-	-	0.02
MSDZ084	0,01	34	0	0.5	2.5	0.18	16	5.6	82	27	125	27	261	43	624	0.061	0.005	813.47	523.962	0.08
MSDZ085	bdl	50	2.9	23.2	58.7	25.3	161	32.5	248	54	144	21	153	17	990	1.05	0.002	-	-	0.79
MSDZ086	bdl	37	0.1	0.7	3.9	0.39	16	5.5	65	22	94	23	189	35	492	0.086	0.004	-	-	0.15
MSDZ087	bdl	20	0.1	0.5	2.4	0.32	13	4.4	58	20	93	21	200	37	468	0.062	0.004	-	-	0.18
MSDZ088	bdl	6	0.1	0.4	0.5	0.31	3	1	12	5	27	7	77	16	155	0.036	0.002	-	-	0.78
MSDZ089	0,01	17	0	0.2	0.8	0.34	3	1.4	15	6	31	8	86	19	188	0.037	0.002	246.603	436.072	0.65
MSDZ090	bdl	3	0.1	0.6	2.3	0.15	9	2.7	28	9	33	6	59	10	162	0.15	0.001	-	-	0.1
MSDZ091	bdl	37	0.7	6.5	10.5	1.31	37	10.9	122	39	158	34	298	47	802	0.124	0.006	-	-	0.2
MSDZ092	bdl	29	0	1.1	3.6	0.3	25	7.7	106	37	152	34	294	51	739	0.083	0.006	-	-	0.1
MSDZ093	bdl	13	0	0.4	0.7	0.28	2	1.1	13	5	26	6	71	14	153	0.031	0.001	-	-	0.66
MSDZ094	bdl	37	0.1	0.9	2.9	0.41	15	5	69	25	119	27	282	52	635	0.052	0.005	-	-	0.19
MSDZ095	bdl	5	0	0.6	1.3	0.67	7	2.4	34	12	66	16	177	36	359	0.041	0.006	-	-	0.67
MSDZ096	bdl	9	0	0.5	1.6	0.96	14	4.3	63	25	113	28	336	55	651	0.042	0.008	-	-	0.62
MSDZ097	bdl	8	0.5	5.6	14.3	0.88	44	9.5	83	19	60	10	77	10	341	0.573	0.001	-	-	0.11
MSDZ098	bdl	7	0.2	2.7	4.9	0.16	19	5	52	17	63	13	117	20	320	0.159	0.002	-	-	0.05
MSDZ099	bdl	7	0.1	1	2.4	0.27	13	3.8	51	18	77	17	154	28	373	0.084	0.003	-	-	0.15

Table 4. *Cont.*

Sample Spot-Name	La	Ce	Pr	Nd	Sm	Eu	Gd	Tb	Dy	Ho	Er	Tm	Yb	Lu	∑REE	Gd/Yb	Lu/Hf	Sm/La_N	Ce/Ce*	Eu/Eu*
MSDZ100	bdl	23	0.1	1.5	4.3	0.43	12	3.3	39	12	44	9	86	15	250	0.14	0.002	-	-	0.18
MSDZ101	bdl	4	0	0.4	1.4	0.25	7	2.9	38	15	75	17	186	35	382	0.039	0.004	-	-	0.24
MSDZ102	bdl	2	0.1	1.5	3.5	0.16	15	3.8	34	8	27	5	44	7	149	0.333	0.001	-	-	0.07
MSDZ103	bdl	8	0.1	2.8	5.9	0.3	21	5.7	56	17	72	15	133	22	360	0.159	0.002	-	-	0.08
MSDZ104	bdl	7	0	0.6	2.4	0.92	13	5.1	66	26	128	30	308	61	648	0.044	0.008	-	-	0.49
MSDZ105	bdl	22	0.1	1.5	4.1	0.41	16	4.6	50	16	63	13	125	21	336	0.128	0.002	-	-	0.15
MSDZ106	bdl	3	0	0.2	1.4	0.32	5	1.6	23	9	41	10	116	20	230	0.041	0.003	-	-	0.38
MSDZ107	bdl	15	0.2	2.9	7.1	0.27	24	7.3	77	26	107	22	203	36	528	0.12	0.004	-	-	0.06
MSDZ108	bdl	3	0.1	2.4	4.7	0.09	16	5.2	53	18	70	15	136	23	347	0.117	0.003	-	-	0.03
MSDZ109	bdl	14	0	0.8	1.7	0.42	7	2.5	37	12	64	14	145	27	325	0.048	0.004	-	-	0.38
MSDZ110	bdl	45	0.6	10.8	18.2	4.34	26	4.3	22	4	10	1	11	1	159	2.476	0.0002	-	-	0.61
MSDZ111	bdl	8	0	0.3	0.7	0.08	7	2.1	26	9	46	11	116	21	247	0.059	0.002	-	-	0.11

Within the LREE suites, the Ce content (2–187 ppm) is dominant. Significantly high Ce content (187 ppm) was obtained in MSDZ055, which has the highest Pr (28.8 ppm), Nd (41.3 ppm), Ti (256 ppm), and Sr (15.99 ppm) contents. The calculated Ce/Ce* anomalies for a few zircons MSDZ003, MSDZ084, and MSDZ089, are 50, 524, and 436, respectively (Table 4). MREE suites show the predominance of Gd contents (3–161 ppm) over those of Nd ($\leq$41.3 ppm), Sm ($\leq$58.7 ppm), and Eu ($\leq$23.50 ppm). The calculated Eu/Eu* (0.03 to <1.33) (Table 4) and normalized plots (Figure 5), mainly show negative anomalies with just a few slightly pronounced positive anomalies (Figure 5a,d,g). The calculated Sm/LaN ratios range from 246 to 1569. Within the HREE suites, Yb contents (2–461 ppm) are generally higher than the contents of Er (3–210 ppm), Dy (4–248 ppm), Lu (1–78 ppm), Ho (1.0–54 ppm), Tm ($\leq$46 ppm), and Tb ($\leq$32.5 ppm). The HREE normalized patterns (Figure 5) generally show an increase from Tb to Lu, except for a few grains (e.g., MSDZ074, MSDZ090, and MSDZ102) whose plots are almost flat. The calculated Gd/Yb and Lu/Hf ratios are <3.0 and <4.1, respectively, with the highest values in MSDZ059 also having the highest Hf/Y ratio ($\approx$274).

4.2. U-Pb Dating

The U-Pb zircon core ages (Table 3, Figures 6 and 7) show Eoarchean to Late Neoproterozoic ^{207}Pb/^{206}Pb (3671 $\pm$ 23 to 637 $\pm$ 24 Ma), ^{207}Pb/^{235}U (3428 $\pm$ 79 to 615 $\pm$ 13 Ma), and ^{206}Pb/^{238}U (3038 $\pm$ 53 to 612 $\pm$ 11 Ma) ages. They are highly heterogeneous, with some different grains having the same age. For plotting and age interpretation purposes, the ^{207}Pb/^{206}Pb dates are used for analyses older than 1000 Ma, whereas the ^{206}Pb/^{238}U dates are used for analyses younger than 1000 Ma. The ^{207}Pb/^{206}Pb data plots for ages greater than 1000 Ma (Figure 7) show the predominance of Middle Paleoproterozoic ages (2050–1993 Ma and 2232–2062 Ma) with the peak at 2130 Ma. Neoarchean age zircons (2797–2531 Ma with the peak at 2700 Ma), in addition to Mesoarchean zircons (3041–2805 Ma) are also abundant. Three grains have ages >3100 Ma (one of Paleo-archean, 3290 Ma, and two of Eo-archean, >3500 Ma). Two grains are of Middle Mesoproterozoic age (>1200 Ma). The ^{206}Pb/^{238}U ages (less than 1000 Ma) for younger zircons show the predominance of the Middle Neoproterozoic ages (Cryogenian) (740–643 Ma), with a few Late Neoproterozoic ages (Ediacarian) (612 and 613 Ma).

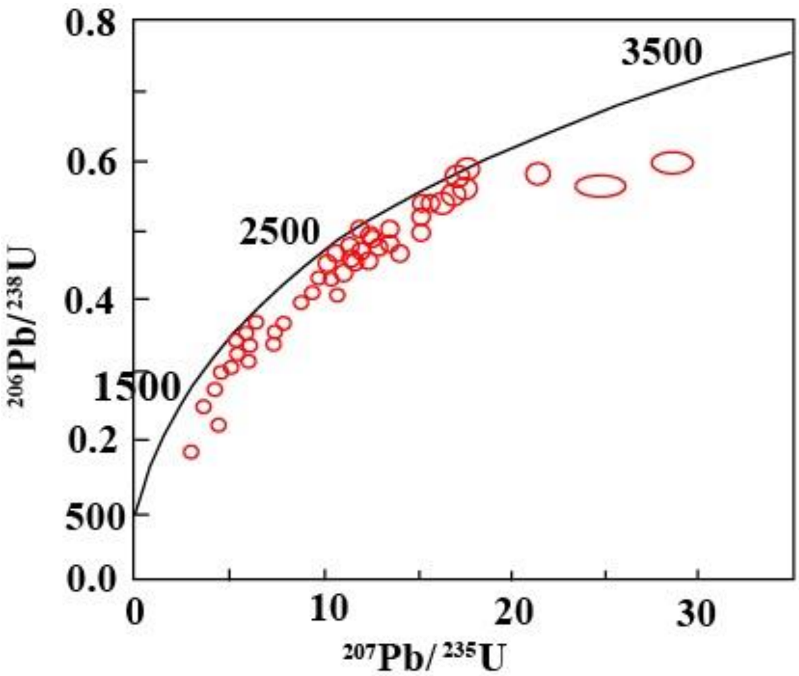

Figure 6. U-Pb discordia diagram for the southern Meiganga detrital zircons.

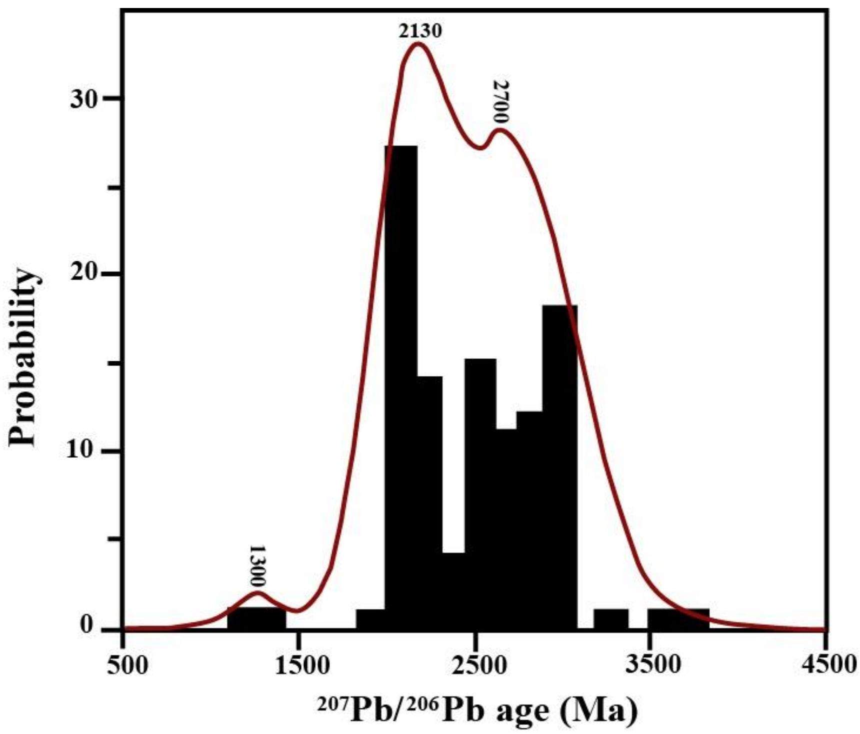

Figure 7. Plot showing the spatial distribution of $^{207}Pb/^{206}Pb$ ages (>1000 Ma) for the southern Meiganga detrital zircons.

5. Discussion

5.1. Zircon Geochemistry, Characterization, Classification, and Environment of Crystallization

The Hf, Y, U, Th, Ti, Nb, Ta, Sr, and REE contents, Th/U ratios, and the Ti-in-zircon temperature are variable, and mainly show a crystallization in different environments. The Th/U ratios distinguish four groups: (1) Th/U < 0.2; (2) Th/U [0.2–0.5]; (3) Th/U [0.5–1.0]; and (4) Th/U > 1.0. They were re-organized into two main groups: (1) igneous affiliated zircons (Th/U ratios $\geq$ 0.2) and (2) metamorphic affiliated zircons (Th/U ratios < 0.2).

5.1.1. Igneous Affiliated Zircons

The trace and rare earth element abundances in the studied igneous affiliated zircons are generally less than those in some zircons found in Cameroon (e.g., [8,9,70]). For example, zircon inclusions in Mayo Kila gem corundum found in the NW region of Cameroon are composed of Hf ($\leq$26,238 ppm), U ($\leq$17,175 ppm), and Th ($\leq$45,584 ppm) [70]. The $\sum$REE contents obtained for detrital zircons occurring with gem corundum in the Mamfe Basin, SW region of Cameroon are up to 1470 ppm [8]. These values are largely greater than those of the studied igneous zircons (Tables 2–4). They can, therefore, be classified as Hf-U-Th-REE-low zircons. Their Hf values are mainly close to those of magmatic zircons found in the western Meiganga gold-bearing placers (cf. [9]), and might show closeness in their crystallization history. The Hf contents in part of the studied zircons are compatible with the values (<11,000 ppm) in zircons crystallized in alkaline magmas [4,71], suggesting a crystallization in alkaline melts. Their plotted data in Figures 4 and 8 show some correlations, as some zircons are plotted together, suggesting a cogenesis and crystallization in the same/similar magma or in different magmas with similar features. This similarity is supported by the closeness of the values of other trace elements, Th/U ratios, and Ti zircon temperatures, and Eu/Eu*.

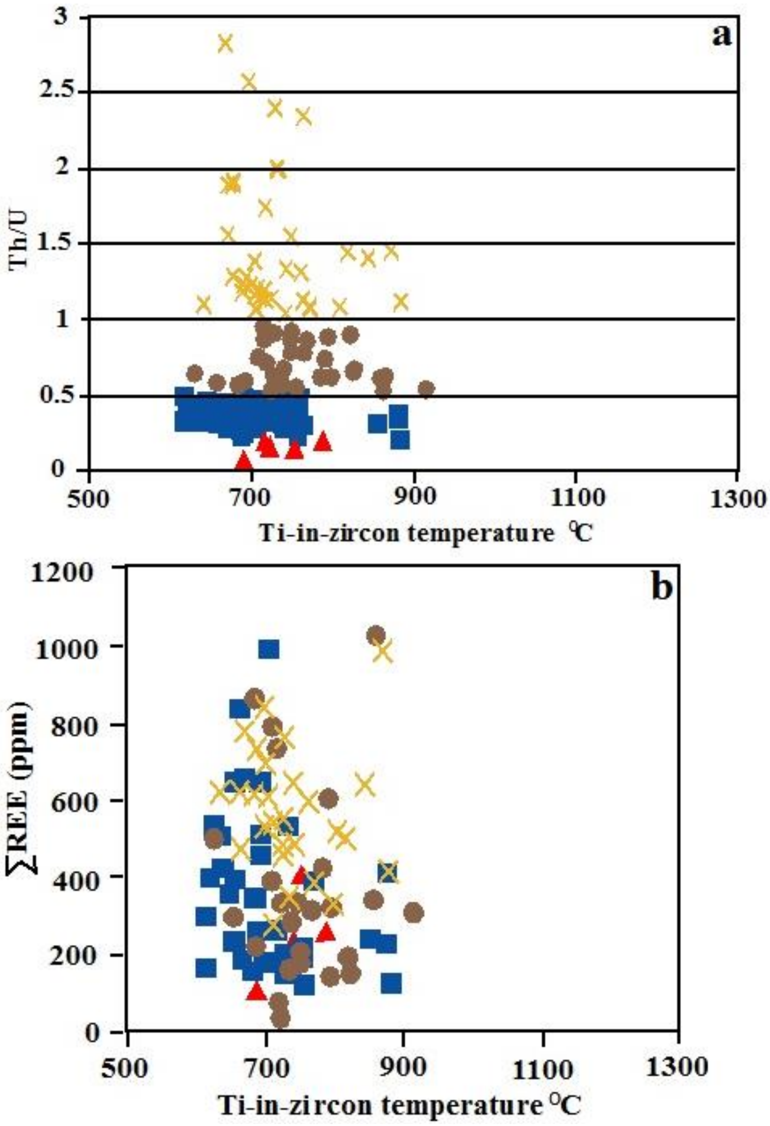

Figure 8. (**a**) Th/U ratio versus Ti-in-zircon temperature (°C) with some grouping of plots, and (**b**) ∑REE (ppm) versus Ti zircon temperature (°C) showing correlations within some zircons from the southern Meiganga gold-bearing placers. Some plots are close while others scattered. Red triangles represent zircon with Th/U < 0.2; blue squares represent zircon with Th/U ratios [0.2 to 0.5]; brown circles represent zircons with Th/U ratios [>0.5 to 1.0]; and stars represent zircons with Th/U > 1.0.

The elemental abundances, Th/U ratios, and Ti-zircon temperatures (617–1180 °C) in the igneous zircons distinguished those with relatively high and relatively low values. Relatively high elemental abundance zircons were probably crystallized in trace elements and REE-enriched melts, with favorable conditions for these elements to substitute Zr in each forming crystal. They are probably crustal-derived zircons, as zircon from crustal rocks generally have elevated contents of some trace elements (notably U, Th, and Y) and REE [4,5]. The relatively high Th (674 ppm), Y (1474 ppm), U (461 ppm), Ti (33 ppm), Nb (25 ppm), and Ta (20 ppm) in MSDZ085, for example, can relate its crystallization in a Y-Th-U-Ti-Nb-Ta-rich magma. The Zr substitution by Nb and Ta during this zircon crystallization was probably governed by Nb, Ta, and REE coupled mechanism (cf. [5]), as this grain also has significant total REE (990 ppm). The relatively high Ti (256 ppm in MSDZ055) may be due to crystallization in Ti-enriched environment with sufficient temperature for Ti to substitute Zr; alternatively, it can be due to Ti-rich mineral inclusion. Relating the high Ti content to a mineral inclusion is difficult, as no inclusion was visualized. The relatively high-elemental zircons are generally from granitoids, as their plots fall essentially in granitoid fields in Figures 9–11. The granitoid origin of those zircons is confirmed by the Y, U, Th, and Yb abundances, largely within the range limit in granitic zircons [4,11,71].

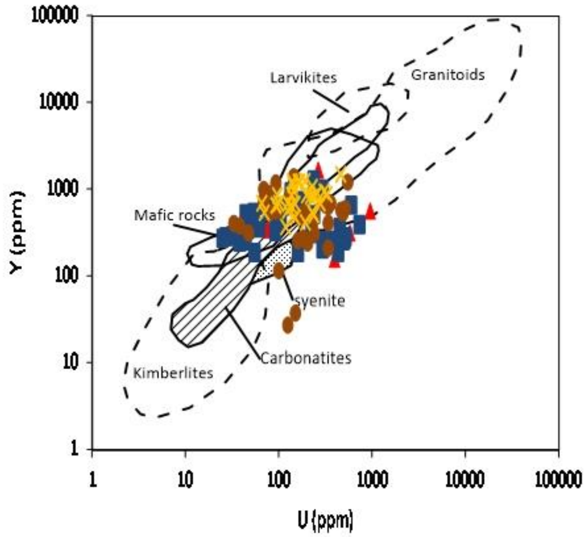

Figure 9. Y versus U plot for southern Meiganga detrital zircons (the lithounit fields are from [4,71]). Red triangles represent zircon with Th/U < 0.2; blue squares represent zircon with Th/U ratios [0.2 to 0.5]; brown circles represent zircons with Th/U ratios [>0.5 to 1.0]; and stars represent zircons with Th/U > 1.0.

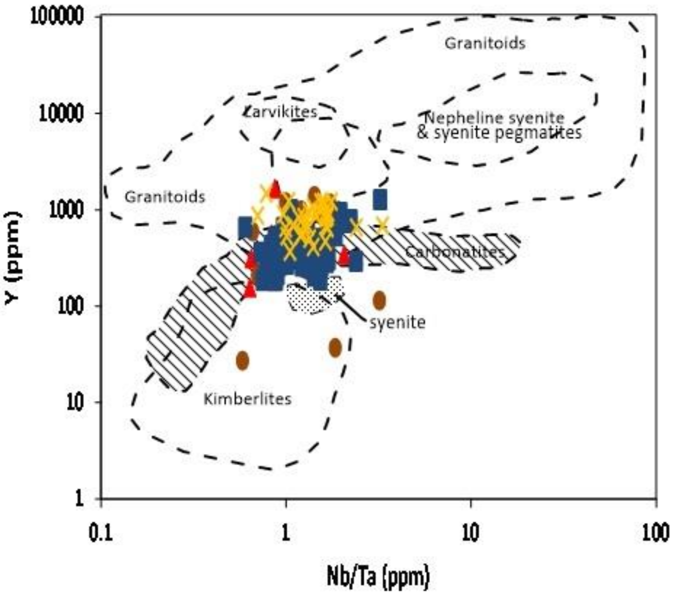

Figure 10. Y versus Nb/Ta plot for southern Meiganga detrital zircons (the lithounit fields are from [4,71]). Red triangles represent zircon with Th/U < 0.2; blue squares represent zircon with Th/U ratios [0.2 to 0.5]; brown circles represent zircons with Th/U ratios [>0.5 to 1.0]; and stars represent zircons with Th/U > 1.0).

Interpretations for very low to low elemental contents in part of the studied zircons can be approached in three ways: (1) elements in those zircon's forming melts are present, but good conditions to ensure that these elements go into their structure are lacking; (2) the depletion or absence of some elements in those zircons' environment of crystallization; or (3) the presence of other accessory minerals (e.g., apatite, xenotime, monazites, allanite, and titanite) [66,72,73] crystallizing in the same melt and competing for REE and other trace elements. The lowest Hf contents in relatively low elemental zircons are within the range limit (4576–6500 ppm) in magmatic zircons found in the western Mamfe corundum gem placers [6–8] and zircon mega-crysts found in alluvial gem corundum deposits associated with alkali basalts (e.g., [74]). These values are also within the range limit (Hf < 9000 ppm) in [10] magmatic zircons crystallized during tectonic rifting. Rifting cannot yet be suggested, as Hf isotopic data are lacking for a detailed interpretation. Zircons from basic and ultrabasic igneous rocks (mantle zircons) are generally depleted in U, Th, Y, and REE [10,75,76]; it is possible that part of the southern Meiganga zircons (e.g., MSDZ016, MSDZ031, MSDZ038, and MSDZ106) were crystallized in mantle source magma(s) as their features, namely U < 30 ppm, Th < 10 ppm, and some plots falling in the mafic rocks field (Figures 9–11), are within the range limit in mantle zircons. The Ti-zircon-temperature (<850 °C) for part of the very low U and Th zircons is less than the temperature (>1300 °C: [77]) for the primary mantle source magma. This temperature difference can complicate the affiliation of part of the very low U and Th zircons to mantle sources. They could be crystals that crystallized at the last stage of cooling mantle source magmas or crystals formed in cooling magmas that originated from the partial fusion of pre-existing mafic rocks. A mafic granulitic origin can be suggested, as part the temperatures are within the range limit (816 ± 12 °C to 798 ± 13 °C) proposed by [78]. Based on the plots of very low to low elemental contents zircons in Figures 9–11, three protosources are distinguished: granitoids, syenites, and mafic rocks.

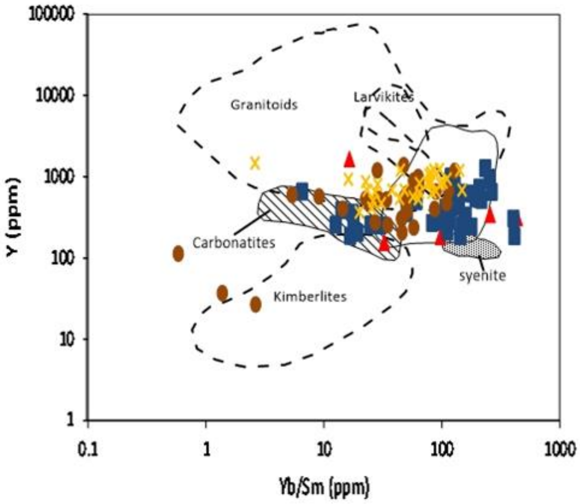

Figure 11. Y versus Yb/Sm plot for southern Meiganga detrital zircons (the lithounit fields are from [4,71]). Red triangles represent zircon with Th/U < 0.2; blue squares represent zircon with Th/U ratios [0.2 to 0.5]; brown circles represent zircons with Th/U ratios [>0.5 to 1.0]; and stars represent zircons with Th/U > 1.0).

5.1.2. Metamorphic Affiliated Zircons

The geochemical features in part of the southern Meiganga detrital zircons are compatible with those of metamorphic zircons grown in equilibrium with garnet (Th/U < 0.07, depletion in REE, Eu/Eu*: 0.24–0.63) (cf. [68]) and crystals grown in equilibrium with an anatectic melt (Th/U < 0.2; relatively trace element-enriched, depleted in MREE, steep REE patterns, positive Ce, and negative Eu anomalies) (cf. [5,9,11,67]). Only one zircon (MSDZ046) with Hf: 9790 ppm, Y: 155 ppm, U: 396 ppm, Th: 26 ppm, Th/U: 0.065, and ∑REE: 98.15 ppm, and Ti temperature: 690 °C, has features close to that of [68] metamorphic zircon grown in subsolidus solution in equilibrium with garnet. This zircon may have crystallized during syn-metamorphic crustal even in low-Th-REE melt. The other zircons (MSDZ015, MSDZ040, MSDZ067, and MSDZ093) have features of zircon grown in equilibrium with anatectic melts, as presented above. The Ti-in-zircon temperatures for these zircons range from 656 ± 60 °C to 778 ± 44 °C, with some values being close to experimental values for granulitic facies metamorphism presented in [78]. Relating their sources to granulitic facies metamorphism is difficult, as some analyses are still needed. MSDZ082, with its positive normalized Pr and Gd plots, is different from the other zircons, as it also has the highest Y (1650 ppm). This grain was plotted in granitoid fields in Figures 9–11, and its other features are close to those of granitoid zircons. It was probably crystallized in an anatectic melt of a granitic composition, as a geochemical feature of a metamorphic zircon grown in equilibrium with anatectic melt does not differ from that of igneous zircons (cf. [5]).

5.2. Detrital Zircon Geochronology and Fingerprinted Magmatic-Metamorphic Events

The recorded U-Pb ages (Table 3, Figures 6 and 7) are mainly heterogeneous with some similarities. The heterogeneity of most of the ages show that they were crystallized at different periods and probably sourced from different protosources and/or source rocks. The crystallization periods of igneous crustal derived zircons, ranging from Eoarchean to Late Neoproterozoic (Figure 7), is composed of three main periods with the following peaks: (1) 1300 Ma of Late Mesoproterozoic; (2) 2130 Ma of Early to Middle Paleoproterozoic; and (3) 2700 Ma of mainly Mesoarchean to Neoarchean. The other magmatic zircon crystallization period is Middle to Late Neoproterozoic (740–612 Ma). This could date four main magmatic episodes linked to crustal fusion; the Mesoarchean to Neoarchean, Early to Middle Paleoproterozoic, Late Mesoproterozoic, and Middle to Late Neoproterozoic events. The obtained group of ages for crustal igneous zircons from the southern Meiganga gold placers show that different magmatic protosources and source rocks provided detritus forming these gold placers. The closeness in ages of some zircons (e.g., MSDZ018: 2801 Ma and MSDZ019: 2802 Ma; MSZD032: 2502 Ma; and MSDZ056: 2503 Ma) may show cogenesis and crystallization at the same time and in the same magma, as their plots overlap (in Figure 12) and fall in the same rock type field (in Figures 9–11).

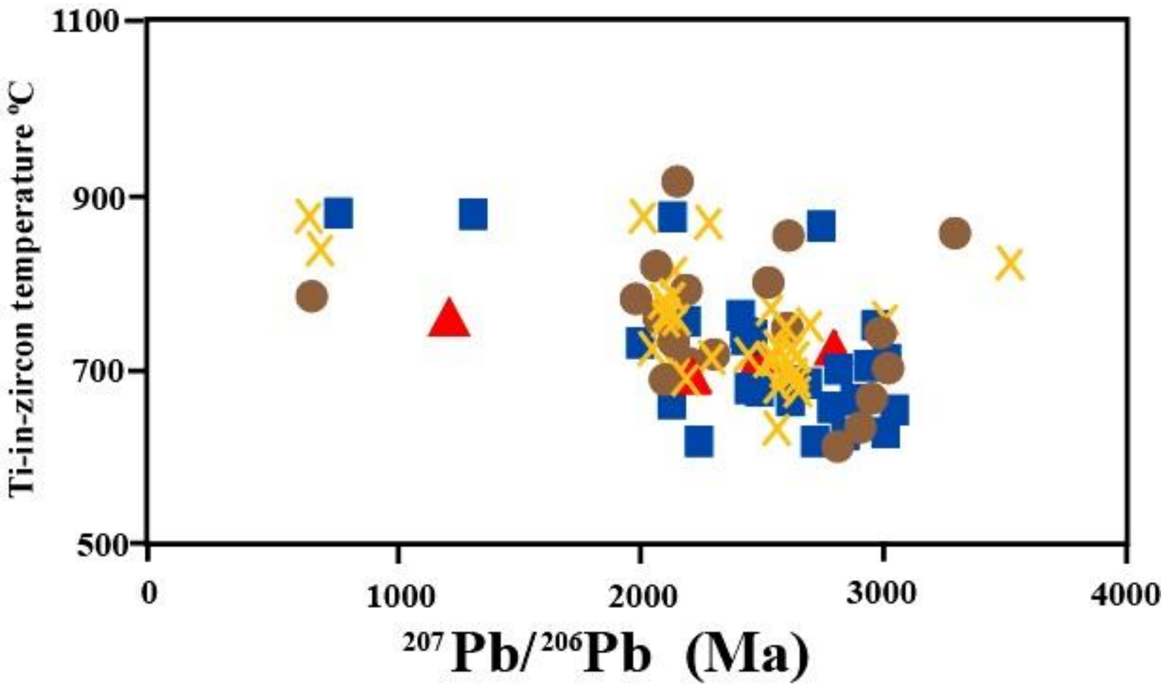

Figure 12. Ti-in-zircon temperature (°C) versus $^{207}Pb/^{206}Pb$ ages (Ma) showing correlations within some zircons from the southern Meiganga gold-bearing placers.

Mafic rock's zircons (MSDZ016: 2999 Ma, MSDZ031: 2797 Ma, MSDZ038: 2795 Ma, and MSDZ106: 2121 Ma), are Early Neoarchean, Late Mesoarchean, and Middle Paleoproterozoic (Rhyacian) mantle source crystals formed probably in magmatic intrusions during crustal opening. The closeness in age between MSDZ031 and MSDZ038 can show that they crystallized at the same time, and probably in the same magma, as their data are plotted together in Figures 2, 4, 7 and 12. Their trace element abundances, and their calculated values are also very close (see Tables 2–4). The Hf contents in this group of zircons (mantle zircons) are all bellow 9000 ppm, and therefore, within the limit proposed by [10] for zircons crystallized during rifting. Rifting and mantle magmatic intrusion cannot be demonstrated easily, as Hf isotopic data are lacking.

The metamorphic zircons $^{207}Pb/^{206}Pb$ ages (2796 Ma, 2559 Ma, 2504 Ma, 2215 Ma, and 2169 Ma) and $^{206}Pb/^{238}U$ age (671 Ma) date three main events: the Neoarchean, Middle Paleoproterozoic, and Middle Neoproterozoic. The Neoarchean and Middle Paleoproterozoic zircons with anatectic melt zircon characteristics, could be grains whose proto-sources underwent metamorphism and partial melting (migmatization). They could be syngenetic zircon crystallized in migrating melts during the Neoarchean and Middle Paleoproterozoic periods. The 671 $\pm$ 12 Ma age of MSDZ015 and its geochemical features are similar to those of zircons grown in equilibrium with garnet, which shows that this syngenetic zircon was crystallized in a garnet-rich rock during Middle Neoproterozoic event, probably the Pan-African orogeny, which affected the Cameroon Mobile Belt. This age is close to those of some Pan-African rocks within the Cameroon Mobile Belt presented in Table 1.

5.3. Age Correlation, Potential Sources Rocks, and Deposition

The southern part of Meiganga from where the studied zircons were sampled is mostly made up of undated biotite-amphibole granites; biotite-amphibole gneisses; biotite granites; biotite-chlorite granitic rocks; and few amphibolites and hornfels (see [53]). With a lack of available data dating those rocks, it is difficult to do a local correlation to locate nearby proto-source(s) and source rocks for the southern detrital zircon Meiganga. However, at local and regional scales, the obtained ages are partly similar to those of zircons occurring in the western Meiganga gold-bearing placer presented in [9] and to the ages of some rocks outcropping in the southwest, northeast, and west of Meiganga, and Congo Craton (see Table 1).

Crustal-derived igneous zircons with ages ranging from 3671 to 612 Ma have some age similarities with those of zircons from some igneous and meta-magmatic rocks found in other parts of Meiganga and in the Congo Craton in South Region of Cameroon (Table 5). For these examples, $^{207}Pb/^{206}Pb$ ages (2605 $\pm$ 14 Ma: MSDZ004, 2988 $\pm$ 16 Ma: MSDZ009, and 2877 $\pm$ 17 Ma: MSDZ077) are close to zircon inherited ages (2602.2 Ma, 2987 Ma, and 2884 Ma) for pyroxene-amphibole-bearing gneiss (TTGs composition: [20,32]) found in the SW of Meiganga. The $^{206}Pb/^{238}U$ ages (612 $\pm$ 11 Ma: MSDZ085 and 619 $\pm$ 11 Ma: MSDZ074) are similar to zircon ages (614.1 $\pm$ 3.9 and 619.8 $\pm$ 9.8 Ma: [37]) for meta-diorite outcropping in the NE of Meiganga. The age of MSDZ043 (643 $\pm$ 11 Ma) is close to that of two micas granite (647 $\pm$ 46 Ma: [21]) outcropping in Doua, west of Meiganga. It is not easy in the current geologic setting to consider these rocks to be source rocks of the southern Meiganga crustal-derived magmatic zircons, as those rocks are often found very far from the sampling points of the studied zircons and their host gold bearing placer. They could be detritus from a nearby undated proto-source and source rock or could be polycyclic detritus from the above rocks.

Mesoarchean, as well as Neoarchean ages of crustal derived igneous zircons are often similar to those from rocks (e.g., charnockite, tonalite, granodiorite, syenite, and granite) found in the Ntem complex (Northern Congo Craton), with just a few links with those from rocks (e.g., garnet-bearing gneiss, meta-quartzite, clinopyroxene syenite, and orthopyroxene-garnet gneiss) of the Nyong Unit (Tables 1 and 5). Early and Middle Paleoproterozoic aged zircons are mainly similar to those from rocks (e.g., amphibolite, charnockite, meta-granodiorite, meta-syenite, and orthopyroxene-garnet gneiss) found within the Nyong Unit (Tables 1 and 5). Their presence in the studied area (within the Cameroon Mobile Belt) shows Archean to Paleoproterozoic inheritance, and post-Archean reworking. The Archean to Paleoproterozic igneous zircons inheritance in some metamorphic rocks found at the west of Meiganga was proven by [20] (see Table 1). Plotted in granitoid field

(Figures 9–11), they could be inherited grains from granite and granodiorite proto-sources with features similar to those of granitoids in the Congo Craton. Those zircons whose plots fall out the various discriminating fields could be inherited grains crystallized in charnockitic and tonalitic magmas, as their ages are close to that of charnockite and tonalite found in the Congo Craton. Those old Archean and Paleoproterozoic rocks were probably reworked with the conservation of some inherited zircons, during the two main tectono-magmatic and metamorphic events (the Eburnean and Pan-African) registered within the Cameroon Mobile Belt.

Table 5. Age correlations between the southern Meiganga detrital zircons and other lithounits in the Congo Craton and in Meiganga.

Age of the Southern Meiganga Detrital Zircons	Age Inheritance and Possible Proto-Source(s) within Rocks in the Congo Craton	Age and Possible Source Rocks in Meiganga
Crustal derived igneous zircons	-	-
Mesoarchean (3041–2805 Ma)	3010–2880 Ma (charnockites, tonalities, clinopyroxene syenites, granodiorites, pyroxene bearing gneiss, and orthopyroxene-garnet gneiss)	2984–2884 Ma: Pyroxene-amphibole-bearing gneiss (TTG composition)
Neoarchean (2796–2531 Ma)	2790–2671 Ma (charnockites, tonalities, granodiorites, High-K granites, garnet-bearing gneiss, and magnetite-bearing quartzites)	≤2602 Ma: pyroxene-amphibole-bearing gneiss (TTG composition)
Early Paleoproterozoic (2486–2302 Ma)	2349 and 2300 Ma (orthopyroxene-garnet gneiss and clinopyroxene syenite)	1999–2339 Ma: pyroxene-amphibole-bearing gneiss (TTG composition) and amphibole-biotite gneiss
Middle Paleoproterozoic (2050–1993 Ma and 2232–2062 Ma)	2126–2000 Ma (meta-syenite, orthopyroxene-garnet gneiss, charnockite, amphibolite, metagranodiorites, and magnetite-bearing quartzite)	
Middle to Late Neoproterozoic (740–612 Ma)	-	614–647 Ma: meta-diorite and two micas granite
Mantle derived zircons 1-Middle Mesoarchean (2999) 2-Early Neoarchean (2797 and 2795 Ma) 3-Middle Paleoproterozoic (2121 Ma)	-	1999–2984 Ma: pyroxene-amphibole-bearing gneiss (TTG composition) and amphibole-biotite gneiss
Metamorphic zircons	-	-
1-Zircon grown in equilibrium with garnet (671 Ma)	-	675 Ma: amphibole-biotite gneiss
2-Zircon grown in equilibrium with an anatectic melt *Neoarchean (2796–2504 Ma) *Middle Paleoproterozoic (2215 and 2169 Ma)	-	≤2884 Ma: Pyroxene-amphibole-bearing gneiss (TTG composition) 1999–2339 Ma: Pyroxene-amphibole-bearing gneiss (TTG composition) and amphibole-biotite gneiss

The age (671 ± 12 Ma) of a metamorphic zircon grown in equilibrium with garnet (MSDZ015) is close to the youngest zircon age (675 Ma: [19]) for amphibole-biotite gneiss found in the west of Meiganga. This rock also hosts Early Paleoproterozic age zircons with some similarities to those of the studied zircons (Table 5). Undated amphibole-biotite gneiss cropping in the south of Meiganga (Figure 1) is the bed-rock of the studied zircon-gold bearing placers. If age extrapolation is possible, it can be suggested that amphibole-biotite gneiss found in the south of Meiganga may be the source rock of part of the detritus forming zircon-gold bearing placers. Indirect sources of the placers can also be pyroxene-amphibole-bearing gneiss, meta-diorite, and two micas granites found within the local settings.

The primary sources of host gold grains are difficult to be directly constrained as gold crystals were not found in placer's rock fragments or in the underlying and surrounding rocks. The depositional periods of the studied zircons are also not easy to constrain. The unconsolidated nature of their host-sediments and their location in streams may suggest post-Neoproterozoic to recent deposition.

6. Conclusions

The southern Meiganga detrital zircon-gold bearing placers are composed of igneous (crustal derived and mantle origin) and metamorphic zircons (grown in equilibrium with garnet and those grown in equilibrium with an anatectic melt) with different histories of crystallization and from mainly different sources.

Crustal derived igneous zircons were crystallized in granitic magmas with some charnockitic and tonalitic affinities during Eoarchean to Late Neoproterozoic periods. Mantle igneous zircons were crystallized from mantle source magmas during Early Neoarchean to Middle Paleoproterozoic times.

The inherited igneous zircons of Mesoarchean to Middle Paleoproterozoic were probably sorted from pyroxene-amphibole-bearing and amphibole-biotite gneiss, with their features similar to those of rocks in the Congo Craton. Late Neoproterozoic zircons, with ages close to those of meta-diorite and two mica granite found in the NE and west of Meiganga, were probably eroded from unidentified nearby rocks formed in the same periods.

Metamorphic zircons grown in equilibrium with garnet were crystallized in low-Th-REE subsolidus solution during the Pan-African syn-metamorphic crustal event. Metamorphic zircons grown in equilibrium with an anatectic melt were probably crystallized during the Neoarchean and Middle Paleoproterozoic in migrated melts from partial fusion of metamorphic protoliths. These inherited zircons were probably sourced from amphibole-biotite gneiss underlying the zircon-gold-bearing placers.

Author Contributions: Conceptualization, N.S.K.; Data curation, A.P.K.; Funding acquisition, N.S.K.; Methodology, P.R.S.; Project administration, N.S.K.; Software, E.A.A.B.; Validation, G.N.; Writing—review and editing, N.S.K. and A.S.V. All authors have read and agreed to the published version of the manuscript.

Funding: The research was partly funded by Professor John Cottle of the Department of Earth Sciences, and the Earth Research Institute, University of California, Santa Barbara, CA, USA, who financed the laboratory analyses.

Acknowledgments: The authors thank John Cottle of the Department of Earth Sciences, and the Earth Research Institute, University of California, Santa Barbara, CA, USA, for financial support and laboratory facilities. We also thank the personnel at the Department Earth Sciences at this same University, as they analyzed the zircons in this study. Our gratitude to Elena Belousova, Tom Andersen, and David Richard Lentz, whose reviews and comments have helped to improve the original manuscript. The authors also extend their gratitude to the two anonymous reviewers whose detailed and constructive comments helped to improve the manuscript.

Conflicts of Interest: The authors declare no conflict of interest.

References

1. Djou, E.S. Prospection des Indices de Minéralisation d'or Dans la Zone de Méiganga-Sud (Nord-Est Cameroun). Master's Thesis, University Yaoundé I, Yaoundé, Cameroon, 2015.
2. Kenna, H.S. Prospection des Indices de Minéralisations d'or Dans la Zone de Méiganga Ouest. Master's Thesis, University Yaoundé I, Yaoundé, Cameroon, 2015.
3. Morton, C.A.; Claoue-Long, C.J.; Hallsworth, C.R. Zircon age and heavy mineral constraints of North Sea Carboniferous sandstones. *Mar. Pet. Geol.* **2001**, *18*, 319–337. [CrossRef]
4. Belousova, A.E.; Griffin, L.W.; O'Reilly, Y.S.; Fisher, I.N. Igneous zircon: Trace element composition as an indicator of source rock type. *J. Miner. Petrol.* **2002**, *143*, 602–622. [CrossRef]
5. Hoskin, P.W.O.; Schaltegger, U. The composition of zircon and igneous and metamorphic petrogenesis. In *Reviews in Mineralogy and Geochemistry*; Mineralogical Society of America: Washington, DC, USA, 2003; Volume 53, pp. 27–55.

6. Kanouo, S.N.; Zaw, K.; Yongue, F.R.; Sutherland, L.F.; Meffre, S.; Njonfang, E.; Ma, C.; Tchouatcha, S.T. U-Pb zircon age constraining the source and provenance of gem-bearing Late Cenozoic detrital deposit, Mamfe Basin, SW Cameroon. *Resour. Geol.* **2012**, *62*, 316–324. [CrossRef]
7. Kanouo, S.N.; Yongue, F.R.; Ekomane, E.; Njonfang, E.; Ma, C.; Lentz, D.R.; She, Z.; Zaw, K.; Venkatesh, A.S. U-Pb ages for zircon grains from Nsanaragati Alluvial Gem Placers: Its correlation to the source rocks. *Resour. Geol.* **2015**, *65*, 103–121. [CrossRef]
8. Kanouo, S.N.; Ekomane, E.; Yongue, F.R.; Njonfang, E.; Zaw, K.; Ma, C.; Ghogomu, R.T.; Lentz, D.R.; Venkatesh, A.S. Trace elements in corundum, chrysoberyl, and zircon: Application to mineral exploration and provenance study of the western Mamfe gem clastic deposits (SW Cameroon, Central Africa). *J. Afr. Earth Sci.* **2016**, *113*, 35–50. [CrossRef]
9. Kanouo, S.N.; Ngueutchoua, G.; Kouske, P.A.; Yongue, F.R.; Venkatesh, A.S. Trace element and U-Pb core age for zircons from western Meiganga gold placer, Cameroon: Their genesis and Archean-Proterozoic sources. *Minerals* **2018**, *8*, 194. [CrossRef]
10. Heaman, L.M.; Bowins, R.; Crocket, J. The chemical composition of igneous zircon suites: Implications for geochemical tracer studies. *Geochem. Cosmochem. Acta.* **1990**, *54*, 1597–1607. [CrossRef]
11. Kanouo, S.N.; Njonfang, E.; Kouské, P.A.; Yongue, F.R.; Ngueutchoua, G. U-Pb zircon age: Preliminary data evaluating the Earth history recorded by two basement rocks (granitic pegmatite and mica-schist) in Mamfe Basin (SW Cameroon, Central Africa). *J. Geol. Geophys.* **2017**, *6*, 1–9. [CrossRef]
12. Cawood, A.P.; Nemchin, A.A. Provenance record of a rift basin: U/Pb ages of detrital zircons from the Perth Basin, Western Australia. *J. Sed. Geol.* **2000**, *134*, 209–234. [CrossRef]
13. Zeh, A.; Gerdes, A.; Klemd, R.; Barton-Jr, M.J. U-Pb and Lu-Hf isotope record of detrital zircon grains from the Limpopo Belt-Evidence for crustal recycling at the Hadean to early-Archean transition. *Geochem. Cosmochem. Acta* **2008**, *72*, 5304–5329. [CrossRef]
14. Gehrels, G. Detrital zircon U-Pb geochronology applied to tectonics. *Annu. Rev. Earth Planet. Sci.* **2014**, *42*, 127–149. [CrossRef]
15. Andersen, T.; Kristoffersen, M.; Elburg, A.M. How far can we trust provenance and crustal evolution information from detrital zircons? A South African case study. *Gondwana Res.* **2016**, *34*, 129–148. [CrossRef]
16. Ganwa, A.A. Les Granitoïdes de Méiganga: Étude Pétrographique, Géochimique, Structurale et Géochronologique: Leur Place dans la Chaîne Panafricaine. Ph.D. Thesis, University Yaoundé I, Yaoundé, Cameroon, 2005.
17. Abbelsalam, G.M.; Liégeois, P.J.; Stern, J.R. The Saharan Metacraton. *J. Afr. Earth Sci.* **2002**, *34*, 119–136. [CrossRef]
18. Ngako, V.; Njonfang, E.; Affaton, P. Pan-African tectonics in northwestern Cameroon: Implication for the history of the western Gondwana. *Gondwana Res.* **2008**, *14*, 509–522. [CrossRef]
19. Ganwa, A.A.; Siebel, W.; Shang, K.C.; Naimou, S.; Ekodeck, G.E. New constraints from Pb-evaporation zircon ages of the Méiganga amphibole-biotite gneiss, Central Cameroon, on Proterozoic crustal evolution. *Int. J. Geosci.* **2011**, *2*, 138–147.
20. Ganwa, A.A.; Klotzli, S.U.; Hauzenberger, C. Evidence for Archean inheritance in the pre-Pan-African crust of Central Cameroon: Insight from zircon internal structure and LA-MC-ICP-MS U-Pb ages. *J. Afr. Earth Sci.* **2016**, *120*, 12–22. [CrossRef]
21. Kepnamou, D.A.; Ganwa, A.A.; Klötzli, S.U.; Hauzenberger, C.; Ngounouno, I.; Naïmou, S. The Pan-African biotite-muscovite granite and amphibole-biotite granite of Doua (Central Cameroon): Zircon features, LA-MC-ICP-MS U-Pb dating and implication on their tectonic setting. *J. Geosci. Geom.* **2017**, *5*, 119–129.
22. Nédélec, A.; Minyem, D.; Barbey, P. High-P-high-T anatexis of Archean tonalitic grey gneisses: The Eseka migmatites, Cameroon. *Precambrian Res.* **1993**, *62*, 191–205. [CrossRef]
23. Penaye, J.; Toteu, S.F.; Tchameni, R.; Van Schmus, W.R.; Tchakounte, J.; Ganwa, A.; Minyem, D.; Nsifa, E.N. The 2.1 Ga West Central African Belt in Cameroon: Extension and evolution. *J. Afr. Earth Sci.* **2004**, *39*, 159–164. [CrossRef]
24. Maurizot, P.; Abessolo, A.; Feybesse, A.; Johan, J.L.; Lecompte, P. *Etude et prospection minière au Sud Ouest Cameroun. Synthèse des travaux de 1978–1985*; Technical Report for BRGM; BRGM: Orléans, France, 1986; CMR 066; p. 274.
25. Tchameni, R.; Mezger, K.; Nsifa, E.; Pouclet, A. Neoarchaean evolution in the Congo Craton: Evidence from K-rich granitoids of the Ntem Complex, Southern Cameroon. *J. Afr. Earth Sci.* **2000**, *30*, 133–147. [CrossRef]
26. Pouclet, A.; Tchameni, R.; Mezger, K.; Vidal, M.; Nsifa, E.; Shang, C.; Penaye, J. Archean crustal accretion at the northern border of the Congo Craton (South Cameroon). The charnockite-TTG link. *Bull. Soc.* **2007**, *5*, 331–342.
27. Nsifa, E.N.; Tchameni, R.; Belinga, S.M.E. *De l'existence de FORMATION Catarchéennes Dans le Complexe Cratonique du Ntem (Sud-Cameroun). Project No. 273, Archean Cratonic Rocks of Africa*; 1993; Volume 23.
28. Tchameni, R.; Pouclet, A.; Mezger, K.; Nsifa, N.E.; Vicat, J.P. Monozircon and Sm-Nd whole rock ages from the Ebolowa greenstone belts: Evidence for the terranes older than 2.9 Ga in the Ntem Complex (Congo craton, South Cameroon). *J. Cameroon Acad. Sci.* **2004**, *4*, 213–224.
29. Chombong, N.N.; Suh, C.E.; Ilouga, C.D.C. New detrital zircon U-Pb ages from BIF-related metasediments in the Ntem Complex (Congo craton) of southern Cameroon, West Africa. *Nat. Sci.* **2013**, *5*, 835–847. [CrossRef]
30. Shang, C.K.; Satir, M.; Siebel, W.; Taubald, H.; Nsifa, E.N.; Westphal, M.; Reitter, E. Genesis of K-rich granitoids in the Sangmelima region, Ntem Complex (Congo craton), Cameroon. *Terra Nostra* **2001**, *5*, 60–63.
31. Shang, K.C.; Liégeois, P.J.; Satir, M.; Frisch, W.; Nsifa, E.N. Late Archaean high-K granite geochronology of the northern metacratonic margin of the Archaean Congo craton, Southern Cameroon: Evidence for Pb-loss due to non-metamorphic causes. *Gondwana Res.* **2010**, *18*, 337–355. [CrossRef]
32. Toteu, S.F.; Van Schmus, W.R.; Penaye, J.; Nyobé, J.B. U-Pb and Sm-Nd evidence for Eburnean and Pan-African high-grade metamorphism in cratonic rocks of southern Cameroon. *Precambrian Res.* **1994**, *108*, 45–73. [CrossRef]

33. Vicat, J.P.; Leger, J.M.; Nsifa, N.E.; Piguet, P.; Nzenti, J.P.; Tchameni, R.; Pouclet, A. Distinction au sein du craton congolais du Sud-Ouest du Cameroun, de deux épisodes doléritiques initiant les cycless orogéniques éburnéen (Paléoprotérozoïque) et panafricain (Néoprotérozoïque). *C. R. Acad. Sci. Paris* **1996**, *323*, 575–582.
34. Shang, K.C.; Satir, M.; Nsifa, N.E.; Liégeois, P.J.; Siebel, W.; Taubald, H. Archaean high-K granitoids produced by remelting of earlier Tonalite–Trondhjemite–Granodiorite (TTG) in the Sangmelima region of the Ntem complex of the Congo craton, southern Cameroon. *Int. J. Earth Sci.* **2007**, *96*, 817–841. [CrossRef]
35. Lasserre, M.; Soba, D. Age Libérien des granodiorites et des gneiss à pyroxènes du Cameroun Méridional. Bull. *BRGM* **1976**, *2*, 17–32.
36. Toteu, S.F.; Penaye, J.; Michard, A. New U-Pb and Sm-Nd data from North-Central Cameroon and its bearing on the pre-Pan-African history of central Africa. *Precambrian Res.* **2001**, *108*, 45–73. [CrossRef]
37. Lerouge, C.; Cocherie, A.; Toteu, F.S.; Penaye, J.; Mile, P.J.; Tchameni, R.; Nsifa, N.E.; Fanning, M.C.; Deloule, E. Shrimp U-Pb zircon age evidence for Paleoproterozoic sedimentation and 2.05 Ga syntectonic plutonism in the Nyong Group, South-Western Cameroon: Consequences for the Eburnean-Transamazonian belt of NE Brazil and Central Africa. *J. Afr. Earth Sci.* **2006**, *44*, 412–427. [CrossRef]
38. Owona, S. Archean-Eburnean and Pan-African Features and Relationships in Their Junction Zone in the South of Yaoundé (Cameroon). Ph.D. Thesis, University Douala, Douala, Cameroon, 2008.
39. Delhal, J.; Ledent, D. *Données Géochronologiques sur le Complexe Calco·Magnésien du Sud-Cameroun*; Technical Report for Department of Geology and Mineralogy of the Royal Museum for Central Africa: Tervuren, Belgium, 1975; pp. 71–76.
40. Tetsopgang, S.; Suzuki, K.; Adachi, M. Preliminary CHIME dating of granites from Nkambe area, northwestern Cameroon. *J. Earth Planet. Sci. Nagoya Univ.* **1999**, *46*, 57–70.
41. Tetsopgang, S.; Suzuki, K.; Njonfang, E. Petrology and CHIME geochronology of Pan-African high K and Sr/Y granitoids in the Nkambe area, Cameroon. *Gondwana Res.* **2008**, *14*, 686–699. [CrossRef]
42. Tagne-Kamga, G. Petrogenesis of the Neoproterozoic Ngondo igneous plutonic complex (Cameroon, west central Africa): A case of late collisional ferro-potassic magmatism. *J. Afr. Earth Sci.* **2003**, *36*, 149–171. [CrossRef]
43. Njiosseu, T.L.E.; Nzenti, P.J.; Njanko, T.; Kapajika, B.; Nédélec, A. New U-Pb zircon ages from Tonga (Cameroon): Coexisting Eburnian-Transmazonian (2.1 Ga) and Pan-African (0.6 Ga) imprints. *C. R. Geosci.* **2005**, *337*, 551–562. [CrossRef]
44. Ganwa, A.A.; Frisch, W.; Siebel, W.; Ekodeck, E.G.; Shang, K.C.; Ngako, V. Archean inheritances in the pyroxene-amphibole-bearing gneiss of the Méiganga area (Central North Cameroon): Geochemical and $^{207}Pb/^{206}Pb$ age imprints. *C. R. Geosci.* **2008**, *340*, 211–222. [CrossRef]
45. Nzenti, J.P.; Barbey, P.; Macaudiere, J.; Soba, D. Origin and evolution of the Late Precambrian high-grade Yaoundé gneisses (Cameroon). *Precambrian Res.* **1988**, *38*, 91–109. [CrossRef]
46. Tchakounté, N.J.; Toteu, F.S.; Van Schmus, R.W.; Penaye, J.; Deloule, E.; Ondoua, M.J.; Houketchang, B.M.; Ganwa, A.A.; White, M.W. Evidence of ca 1.6 Ga detrital zircon in Bafia group (Cameroon): Implication for chronostratigraphy of the Pan-African Belt north of the Congo craton. *C. R. Geosci.* **2007**, *339*, 132–142. [CrossRef]
47. Ganwa, A.A.; Frisch, W.; Siebel, W.; Shang, C.K. Geochemistry of magmatic rocks and time constraints on deformational phases and shear zone slip in the Méiganga area, Central Cameroon. *Int. Geol. Rev.* **2011**, *53*, 759–784. [CrossRef]
48. Ganwa, A.A.; Klötzli, S.U.; Kepnamou, D.A.; Hauzenberger, C. Multiple Ediacaran tectono-metamorphic events in the Adamawa-Yadé Domain of the Central Africa Fold Belt: Insight from the zircon U-Pb LAM-ICP-MS geochronology of the metadiorite of Meiganga (Central Cameroon). *Geol. J.* **2018**, 1–14. [CrossRef]
49. Shang, C.K.; Siebel, W.; Satir, M.; Chen, F.; Mvondo, J.O. Zircon Pb-Pb and U-Pb systematics of TTG rocks in the Congo craton: Constraints of crustal formation, crystallization and Pan-African lead loss. *Bull. Geosci.* **2004**, *79*, 205–219.
50. Kornprobst, J.; Cantagrel, J.M.; Fabries, J.; Lasserre, M.; Rollet, M.; Soba, D. Existence in Cameroon of a Pan-African or older alkaline magmatism, the nepheline syenite with mboziite of Nkonglong; comparison with the known alkaline rocks of the same region. *Bull. Soci. Geol. France* **1976**, *18*, 1295–1305. [CrossRef]
51. Tchameni, R.; Mezger, K.; Nsifa, N.E.; Pouclet, A. Crustal origin of Early Proterozoic syenites in the Congo craton (Ntem complex), South Cameroon. *Lithos* **2001**, *57*, 23–42. [CrossRef]
52. Toteu, S.F.; Penaye, J.; Poudjom Djomani, Y.H. Geodynamic evolution of the Pan-African belt in Central Africa with special reference to Cameroon. *Can. J. Earth Sci.* **2004**, *41*, 73–85. [CrossRef]
53. Lassere, M. Carte Géologique de Reconnaissance à l'échelle du 1/500 000 Territoire du Cameroun, Ngaoundéré Est. Dir. Mines Géol. Cameroun, Yaoundé, 1 carte et notice. 1961.
54. Parfenoff, A.; Pomerol, C.; Tourenq, J. *Les Minéraux en Grains. Méthodes D'étude et Détermination*; Masson et Cie Edition: Paris, France, 1970.
55. Kanouo, S.N. Geology of the Western Mamfe Corundum Deposits, SW Region Cameroon: Petrography, Geochemistry, Geochronology, Genesis, and Origin. Ph.D. Thesis, University Yaoundé I, Yaoundé, Cameroon, 2014.
56. Cottle, J.M.; Waters, D.J.; Riley, D. Metamorphic history of the South Tibetan Detachment System, Mt. Everest region, revealed by RSCM thermometry and phase equilibria modelling. *J. Metamorph. Geol.* **2011**, *29*, 561–582. [CrossRef]
57. Cottle, J.M.; Burrows, A.J.; Kylander-Clark, A.; Freedman, P.A.; Cohen, R. Enhanced sensitivity in laser ablation multi-collector inductively coupled plasma mass spectrometry. *J. Anal. At. Spectrom.* **2013**, *28*, 1700–1706. [CrossRef]

58. Kylander-Clark, A.R.C.; Hacker, B.R.; Cottle, J.M. Laser-ablation split-stream ICP petrochronology. *Chem. Geol.* **2013**, *345*, 99–112. [CrossRef]
59. Paton, C.; Woodhead, J.; Hellstrom, J.; Hergt, J.; Greig, A.; Maas, R. Improved laser ablation U-Pb zircon geochronology through robust down hole fractionation correction. *Geochem. Geophys. Geosyst.* **2010**, *11*, 1–36. [CrossRef]
60. Wiedenbeck, M.; Alle, P.; Corfu, F.; Grin, W.; Meier, M.; Oberli, F.; Von Quadt, A.; Roddick, J.; Spiegel, W. Three natural zircon standards for U-Th-Pb, Lu-Hf, trace element and REE analyses. *Geostand. Newslett.* **1995**, *19*, 1–23. [CrossRef]
61. Jackson, S.; Pearson, N.; Griffin, W.; Belousova, E. The application of laser ablation-inductively coupled plasma-mass spectrometry to in situ U/Pb zircon geochronology. *Chem. Geol.* **2004**, *657*, 47–69. [CrossRef]
62. Ludwig, K. *User's Manual for Isoplot 2.4: A Geochronological Toolkit for Microsoft Excel*; Berkeley Geochronology Center: Berkeley, CA, USA, 2012.
63. Vermeesch, P. On the visualisation of detrital age distributions. *Chem. Geol.* **2012**, *312–313*, 190–194. [CrossRef]
64. Steiger, R.; Jager, E. Subcommission on geochronology: Convention on the use of decay constants in geo and cosmochronology. *Earth Planet. Sci. Lett.* **1977**, *36*, 359–362. [CrossRef]
65. Konzett, J.; Armstrong, R.A.; Sweeny, R.J.; Compston, W. The timing of Marid suite metasomatism in the Kaapvaal mantle: An ion probe study of zircons from Marid xenoliths. *Earth Planet. Sci. Lett.* **1998**, *160*, 133–145. [CrossRef]
66. Kirkland, C.L.; Smithies, R.H.; Taylor, R.J.M.; Evans, N.; McDonald, B. Zircon Th/U ratios in magmatic environs. *Lithos* **2015**, *212–215*, 397–414. [CrossRef]
67. Hiess, J.; Nutman, A.P.; Bennett, V.C.; Holden, P. Ti-in-zircon thermometry applied to contrasting Archean metamorphic and igneous systems. *Chem. Geol.* **2008**, *247*, 323–338. [CrossRef]
68. Rubatto, D. Zircon trace element geochemistry: Partitioning with garnet and link between U-Pb ages and metamorphism. *Chem. Geol.* **2002**, *184*, 123–138. [CrossRef]
69. McDonough, F.W.; Sun, S.S. The composition of the Earth. *Chem. Geol.* **1995**, *120*, 223–253. [CrossRef]
70. Mbih, P.K.; Sebastien Meffre, S.; Yongue, F.R.; Kanouo, S.N.; Jay, T. Chemistry and origin of the Mayo Kila sapphires, NW region Cameroon (Central Africa): Their possible relationship with the Cameroon volcanic line. *J. Afr. Earth Sci.* **2016**, *118*, 263–273. [CrossRef]
71. Veevers, J.J.; Belousova, A.E.; Saeed, A.; Sircombe, K.; Cooper, F.A.; Read, E.S. Pan-Gondwanaland detrital zircons from Australia analyzed for Hf-isotopes and trace elements reflect an ice-covered Antarctic provenance of 700–500 Ma age, TDM of 2.0–1.0 Ga, and alkaline affinity. *Earth Sci. Rev.* **2006**, *76*, 135–174. [CrossRef]
72. Gromet, P.L.; Silver, T.L. Rare earth element distributions among minerals in a granodiorite and their petrogenetic implications. *Geochem. Cosmochem. Acta.* **1983**, *47*, 925–939. [CrossRef]
73. Pettke, T.; Audétat, A.; Schaltegger, U.; Heinrich, C.A. Magmatic-to-hydrothermal crystallization in the W-Sn mineralized Mole Granite (NSW, Australia): Part II: Evolving zircon and thorite trace element chemistry. *Chem. Geol.* **2005**, *220*, 191–213. [CrossRef]
74. Abduriyim, A.; Sutherland, L.F.; Belousova, A.E. U-Pb age and origin of gem zircon from the New England sapphire fields, New South Wales, Australia. *Aust. J. Earth Sci.* **2012**, *59*, 1067–1081. [CrossRef]
75. Belousova, A.E.; Griffin, L.W.; Pearson, J.N. Trace element composition and cathodoluminesence properties of southern African kimberlitic zircons. *Mineral. Mag.* **1998**, *62*, 355–366. [CrossRef]
76. Hoskin, P.W.O.; Black, L.P. Metamorphic zircon formation by solid-state recrystallization of protolith ignous zircon. *J. Met. Petrol.* **2000**, *18*, 423–439. [CrossRef]
77. Green, H.D.; Falloon, J.T.; Eggins, M.S.; Yaxley, M.G. Primary magmas and mantle temperatures. *Eur. J. Mineral.* **2001**, *13*, 437–451. [CrossRef]
78. Pattison, M.R.D.; Chacko, T.; Farquhar, J.; Mcfarlane, M.R.C. Temperatures of granulite-facies metamorphism: Constraints from experimental phase equilibria and thermobarometry corrected for retrograde exchange. *J. Petrol.* **2003**, *44*, 867–900. [CrossRef]